Surface Passivation with Phenethylammonium Iodide (PEAI) to Enhance Efficiency in Perovskite Solar Cell

Bona Woliyi Hirpho

A Thesis Submitted to Department of Materials Science and Engineering

College of Mechanical, Chemical and Materials Engineering

Presented in Partial Fulfillment of the Requirement for the Degree of Master's in Materials Science and Engineering

Office of Graduate Studies

Adama Science and Technology University

June, 2025

Adama, Ethiopia

Surface Passivation with Phenethylammonium Iodide (PEAI) to Enhance Efficiency in Perovskite Solar Cell

Mr. Bona Woliyi Hirpho

Advisor: Dr. Temesgen Debelo Desissa (Ph.D.)

Co-Advisor: Dr. Newayemedhin Aberra Tegegne (Ph.D.)

A Thesis Submitted to Department of Materials Science and Engineering

College of Mechanical, Chemical and Materials Engineering

Presented in Partial Fulfillment of the Requirement for the Degree of Master's in Materials Science and Engineering

Office of Graduate Studies

Adama Science and Technology University

June, 2025

Adama, Ethiopia

DECLARATION

I hereby declare that this Master Thesis entitled **"Surface Passivation with Phenethylammonium Iodide (PEAI) to Enhance Efficiency in Perovskite Solar Cell"** is my original work. That is, it has not been submitted for the award of any academic degree, diploma, or certificate in any other university. All sources of materials that are used for this thesis have been duly acknowledged through citation.

_____	_____	_____
Name of the Student	Signature	Date

RECOMMENDATION

I/we, the advisor(s) of this thesis, hereby certify that I/we have read the revised version of the thesis entitled "**Surface Passivation with Phenethylammonium Iodide (PEAI) to Enhance Efficiency in Perovskite Solar Cell**" prepared under my/our guidance by Bona Woliyi Hirpho submitted in partial fulfillment of the requirements for the degree of Master's of Science in **Materials Science and Engineering**

Therefore, I/we recommend the submission of revised version of the thesis to the Department following the applicable procedures.

Major Advisor	Signature	Date
Newayemedhin Aberra Tegegne		16/06/2025
Co-advisor	Signature	Date

APPROVAL SHEET

I/we, the advisors of the thesis entitled **"Surface Passivation with Phenethylammonium Iodide (PEAI) to Enhance Efficiency in Perovskite Solar Cell"** and developed by Bona Woliyi Hirpho hereby certify that the recommendation and suggestions made by the board of examiners are appropriately incorporated into the final version of the thesis.

Major Advisor	Signature	Date

We, the undersigned, members of the Board of Examiners of the thesis by Bona Woliyi Hirpho have read and evaluated the thesis entitled **"Surface Passivation with Phenethylammonium Iodide (PEAI) to Enhance Efficiency in Perovskite Solar Cell"** and examined the candidate during the open defense. This is, therefore, to certify that the thesis is accepted for partial fulfillment of the requirement of the degree of Master of Science in Material science and engineering.

Chairperson	Signature	Date
Internal Examiner	Signature	Date
External Examiner	Signature	Date

Finally, approval and acceptance of the thesis are contingent upon the submission of its final copy to the Office of Postgraduate Studies (OPGS) through the Department Graduate Council (DGC) and School Graduate Committee (SGC).

Department Head	Signature	Date
College Dean	Signature	Date
Office of Postgraduate Studies, Dean	Signature	Date

ACKNOWLEDGMENT

Above all, I want to address my thanks to my research advisors, Dr. Temesgen Debelo Desissa and Dr. Newaymedhin Abera Tegegn, for their continues support throughout my thesis work. Your insightful perspectives, expert guidance, and constant motivation have been invaluable. I wish to express my extended gratitude to my colleagues, Mr. Biruk Alebachew Seid for his support, collaboration, guidance, advice and being available for me at any time I need him throughout this project. This endeavor would not have been possible without your involvement, encouragement, and collaborative efforts. Your readiness to share resources, exchange ideas, and offer valuable feedback at every stage of the study was crucial for conducting a thorough analysis.. Additionally, your professionalism, drive, and passion for the project industry have been a source of inspiration for me. I would like to express my gratitude to ASTU for this opportunity, as well as to all MSE stuff specially, Dr. Gebisa Bekele, Dr. Fekadu Gochole, Dr. Fetene Fufa, Dr. Dinsefa Mensur and all the ARA of the Materials Science and Engineering program, Mr. Demeke Tesfaye, Biruk Sisay and Eyob Adane. I would like to convey my heartfelt appreciation to Professor Fikadu Gashaw, who leads the Physics department at Addis Ababa University (4 Kilo Campus), for his support during my thesis work. The Institute has played a crucial role by providing the essential resources and facilities needed for the success of my research. Lastly, I am grateful to my family, classmates, and everyone who has offered me support in any form.

TABLE OF CONTENTS

ACKNOWLEDGMENT I
TABLE OF CONTENTS II
LIST OF TABLES IV
LIST OF FIGURES V
LIST OF ABBREVIATION VII
CHAPTER ONE 1
1. INTRODUCTION 1
1.1 Background of study 1
1.2. Statement of problem 4
1.3 Objectives 4
1.3.1 General objective 4
1.3.2 Specific objectives 4
1.4 Significance of the study 5
1.5 Scope of the study 6
CHAPTER TWO 7
2. LITERATURE REVIEW 7
2.1 Solar energy 7
2.2 Photovoltaic technology 8
2.3 Perovskite structure 9
2.4 Perovskite solar cells (PSCs) 11
2.4.1 Basic working principles of perovskite solar cells 12
2.5 Photovoltaic parameters 13
2.5.1 Short circuit current density (J_{sc}) 13
2.5.2. Open circuit voltage (V_{oc}) 13
2.5.3 Fill factor (FF) 13
2.5.4 Power conversion efficiency (PCE) 14
2.6 Materials systems in PSCs 14
2.6.1 Structural and photovoltaic properties of single-cation lead halide perovskites 15
2.6.2 Advantages of dual and triple cation perovskites for solar cells 19
2.7 Electron transport materials (ETMs) 22
2.8 Hole transport materials in PSC 24
2.9 Challenges in perovskite solar cells 26
2.9.1 Stability 26
2.9.2 Hysteresis 29
2.10 Interface engineering 30

CHAPTER THREE 33
3. EXPERMENTAL METHODOLOGY 33
3.1 Materials and Chemicals 33
3.1.1 Chemicals 33
3.1.2 Materials 33
3.2 Preparation of perovskite solution and thin film 33
3.3 Preparation of PEAI solution 34
3.4 Surface passivation of triple cation perovskite 34
3.5 Preparation of MeO-2PACz solution 35
3.6 Device fabrication 35
3.7 Material characterizations 36
CHAPTER FOUR 37
4. RESULTS AND DISCUSSION 37
4.1 XRD data analysis 37
4.2 UV-Vis spectroscopy measurement 39
4.3 Photoluminescence measurement 40
4.4 Electroluminescence measurement 42
4.5 Scanning electron microscopy image of perovskite film 44
4.6 Photovoltaic performance of devices 45
4.7 External quantum efficiency analysis 46
Conclusion 48
Reference 49

LIST OF TABLES

Table 1. Summary of device geometries and performance of triple cation based perovskite solar cells 32
Table 2. Crystalline size for passivated film 38
Table 3. Crystalline size for control film 38
Table 4. Summary of performance of control and PEAI passivated PSCs device. 46

LIST OF FIGURES

Figure 1. Fossil fuel based (a) and renewable energy source (b) 8
Figure 2. Perovskite crystal structure 9
Figure 3. Perovskite crystalline system 10
Figure 4. The solar cell efficiency trend over a years 11
Figure 5. Work principles of Perovskite Solar Cells 12
Figure 6. (a) Current-voltage (J-V) characteristics illustrating the performance of a solar cell. (b) The corresponding equivalent circuit model, where Rsh represents the shunt resistance associated with leakage currents, and RS denotes the series resistance arising from impediments to current flow within the cell 14
Figure 7. Crystal structure of $CsPbI_3$ (a), along with the temperature induced phase transitions that alter its structural configuration as the material transitions between different crystallographic phases 17
Figure 8. Surface morphology of the $FAPbI_3$ perovskite film derived from a non-stoichiometric (NS) precursor solution is presented in the SEM image (a); the corresponding X-ray diffraction (XRD) pattern of the NS perovskite is shown in (b); the optical band gap determined via Tauc's plot is illustrated in (c); three-dimensional topography of the NS perovskite active layer without octylammonium iodide (OAI), obtained using atomic force microscopy (AFM), is depicted in (d); surface potential measurements conducted by Kelvin probe force microscopy (KPFM) in the dark and under white light illumination on the same 3D NS perovskite film are shown in (e) and (f), respectively 18
Figure 9. a) 3D cubic crystal structure representing the ideal perovskite with the general formula ABX_3; (b) a schematic layout of the inverted perovskite solar cell architecture comprising ITO/hybrid electron transport layer (ETL)/perovskite/hole transport layer (HTL)/metal electrode; and (c) a conceptual illustration of charge carrier dynamics along with a simplified flat-band energy level diagram of the perovskite solar cell as modeled and analyzed in this study 24
Figure 10. Flowchart illustrating the classification of hole-transporting materials (HTMs) ... 26
Figure 11. Source of instability in perovskite materials and perovskite solar cells 27
Figure 12. Moisture-induced degradation of $MAPbI_3$ perovskite 27
Figure 13. Intrinsic stability of perovskites. (A) Illustration of the tolerance factor (t) as a function of the effective ionic radius, indicating the likelihood of different structural phases (X. Li et al., 2016). (B) technique of mixing of A-site species (Mazumdar et al., 2021). (C) and (D) Defect tolerance of $MAPbI_3$ as predicted by density functional theory (DFT) calculations (Mazumdar et al., 2021). (C) formation energies in three different conditions, from left to right-I-rich/Pb-poor, neutral and Pb-rich/I-poor. (D) Transition energy

levels for intrinsic acceptor (left) and donor (right) point defects. (E) Correlation between the valence band maximum and the I/Pb ratio in $MAPbI_3$ films, as determined by X-ray photoelectron spectroscopy (XPS) 28
Figure 14. The PSCs recombination processes 30
Figure 15. Preparation procedure of Triple cation perovskite solution and film 34
Figure 16. Surface Passivation of Triple Cation Perovskite film 35
Figure 17. Device fabrication procedure 36
Figure 18. a) XRD pattern of control and PEAI passivated perovskite film, b) the peak position shift of perovskite films. 38
Figure 19. a) UV-vis absorbance spectra of perovskite films grown on ITO. b) Transmittance spectra of perovskite films grown on ITO. c) Tauc plots 40
Figure 20. Photoluminiscence of control and PEAI passivated perovskite film. 41
Figure 21. The schematic of an EL sample preparation by sandwiching $Cs_{0.05}(MA_{0.02}FA_{0.98})_{0.95}Pb(I_{0.98}Br_{0.02})_3$ in between ITO-coated glass plates and Cu electrode..42
Figure 22. a) Electroluminescence spectrum of passivated and non-passivated perovskite film b) Electroluminescence imaging for control, and c) passivated devices 43
Figure 23: SEM images of perovskite films: (a) Control, (b) PEAI-treated. 44
Figure 24. J-V curves of control and PEAI treated PSCs devices 45
Figure 25. The external quantum efficiency (EQE) spectra of both the control and PEAI passivated PSCs. 47

LIST OF ABBREVIATIONS

AM1.5G	Air Mass 1.5 Global
CB	Chlorobenzene
CBM	Conduction Band Minimum
DI	Deionized
DMF	Dimethylformamide
DMSO	Dimethyl Sulfoxide
Eg	Band Gap Energy
EAI	Ethylammonium Iodide
EL	Electroluminiscence Spectroscopy
EQE	External Quantum Efficiency
ETL	Electron Transport Layer
FA	Formamidinium
FAMA	Formamidinium Methylammonium
FAPbI	Formamidinium Lead Iodide
FF	Fill Factor
FTO	Fluorine-Doped Tin Oxide
FWHM	Full Width at Half Maximum
HI	Hysteresis Index
HOMO	Highest Occupied Molecular Orbital
HTL	Hole Transport Layer
ISC	Short-Circuit Current
IE	Ionization Energy
IPA	Isopropyl Alcohol
ITO	Indium Tin Oxide
JSC	Short-Circuit Current Density
J-V	Current Density-Voltage
LED	Light-Emitting Diode
MA	Methylammonium
MAPI	Methylammonium Lead Iodide
MPP	Maximum Power Point
PAI	Phenylammonium Iodide
PCE	Power Conversion Efficiency

PEAI	Phenylethylammonium Iodide
PL	Photoluminescence
PSC	Perovskite Solar Cell
PV	Photovoltaic
RS	Series Resistance
RSh	Shunt Resistance
RH	Relative Humidity
RT	Room Temperature
SQ	Shockley-Queisser
SRH	Shockley-Read-Hall
TCO	Transparent Conducting Oxide
UV	Ultraviolet
V_{OC}	Open-Circuit Voltage
VBM	Valence Band Maximum
XRD	X-ray diffraction
2D	2-Dimensional
3D	3-Dimensional

ABSTRACT

Perovskite solar cells (PSCs) have attracted significant attention for their impressive power conversion efficiencies (PCEs) in recent years However, further improvements in device performance remain a major challenge. One of the key limiting factors is the presence of surface defects in the perovskite layer, which promote nonradiative recombination and cause carrier transport losses, particularly at the interface between the perovskite and the electron-selective contact layer (e.g., C_{60}). To address these issues, interface engineering of the perovskite absorber layer has emerged as a widely adopted and effective strategy for minimizing interfacial losses and enhancing overall device efficiency. Organic ammonium halide salts are commonly used as surface modifiers in the form of 2D perovskites to create 2D/3D bilayer structures that enhance efficiency and stability. This thesis investigates the use of phenethylammonium iodide (PEAI) as a 2D passivation for surface passivation of triple-cation perovskite materials, specifically $Cs_{0.05}(MA_{0.02}FA_{0.98})_{0.95}Pb(I_{0.98}Br_{0.02})_3$. We demonstrate that PEAI passivation effectively reduces surface defects, suppresses nonradiative recombination, and leads to enhanced charge carrier dynamics. As a result, devices treated with PEAI achieve a PCE of 20.6%, compared to 18.9% for the control device. This overall improvement in PCE primarily arises from increases in open-circuit voltage (Voc) and fill factor (FF), attributed to the beneficial passivation effect of the 2D layer. This is further supported by enhanced photoluminescence (PL) and electroluminescence (EL) emission. In contrast, the short-circuit current density (Jsc) remains nearly unchanged, consistent with the unaltered optical absorption and external quantum efficiency (EQE) spectra. Despite their benefits, 2D perovskite layers can damage the underlying 3D perovskite during post-annealing and introduce exciton transport barriers due to degradation of the 2D itself. To avoid these issues, we directly applied phenethylammonium iodide (PEAI) without post-annealing. This prevents the formation of a separate 2D phase and preserves efficient charge transport in the 3D structure, while still enhancing device performance.

Keywords: perovskite solar cell, phenethylammonium iodide, surface passivation, nonradiative recombination, 2D perovskite, power conversion efficiency

CHAPTER ONE

1. INTRODUCTION

1.1 Background of study

The increasing global energy demand and the depletion of fossil fuels have accelerated the finding for alternative energy resources. Various renewable energy technologies, including wind, hydroelectric, geothermal, and conventional solar power, are currently under investigation (Ang et al., 2022); however, inorganic-organic perovskite solar cells (PSCs) have attracted considerable research central goal as a promising PV technology (R. He et al., 2021). Perovskite materials demonstrate high potential in different optoelectronic devices, including photovoltaics, light-emitting diodes, photodetectors, and lasers (Jeon et al., 2018). Among these applications, the enhancement of solution processed perovskites in PVs is noteworthy; due to their super light absorption and exciton transport properties have led to PCEs surpassing 27% (Jiang et al., 2019; Li et al., 2019).

This elevated attention is attributed to their production cost effectiveness and rapidly improving PCEs, which now surpass 27% (Sharma et al., 2022). However, it is important to emphasize that even with these remarkable PCE values, they still do not reach the Shockley-Queisser limit (Zhou et al., 2021). As short circuit current density (Jsc) approaches its theoretical limits (~ 26 mA cm^{-2}) and the fill factor (FF) achieves high levels exceeding 80% (Liu et al., 2019; Yoo et al., 2019). Significant efforts are being dedicated to enhancing the open-circuit voltage (Voc) of PSCs. To further enhance the efficiency of PSCs devices and facilitate their widespread implementation for sustainable and affordable energy solutions, numerous research strategies are being actively pursued, although certain obstacles persist. Along with compositional engineering and the modulation of the work function of the charge transport layers, (Hu et al., 2018; Wang et al., 2017), passivation of imperfection is recently a prevalent and efficient approach to reduce Voc loss, given the strong correlation between nonradiative recombination of charge and the Voc of PSCs. Notably, nonradiative recombination cause a significant challenge that requiring in-depth study (Tao et al., 2024), as the passivation of detrimental defects at perovskite surfaces and/or grain boundaries is essential to minimize the formation of undesirable

recombination centers that trap photo generated charge carriers (Seshaiah & Kim, 2024).

Various research technique are being extensively explored to improve the performance of perovskite devices. These strategies encompass the improvement of perovskite material composition, interface engineering, antisolvent methods for film crystallization control, and perovskite surface passivation. Among the various surface passivation strategies reported are thin protective capping layer (Bi et al., 2017), Lewis bases (Wang et al., 2020), low-dimensional perovskite (Liu et al., 2020), and organic ammonium halide salts (Akin et al., 2021). These surface Passivation techniques can be strategically implemented at different interfaces of PSCs device, including at the HTL/perovskite layer, perovskite layer/ETL, HTL/anode, ETL/cathode, and also at grain boundaries within the perovskite layer.

A central objective of perovskite surface passivation is to suppress surface defects (Fu et al., 2020) and enhance operational stability of perovskite devices (Gu et al., 2021). These passivation materials can be classified into two categories: those that modify only the perovskite surface without forming any new perovskite layer on top of the 3D perovskite (Wu et al., 2022), and those that form a 2D perovskite layer on top of the 3D perovskite layer (Yu et al., 2022). Organic ammonium halide salts offer a versatile approach, that capable of enhancing the in-situ formation of 2D/3D perovskite heterostructures to enhance both device stability and efficiency. Although post-annealing treatments are applied most of time to enhance crystallinity, some studies have reported that such thermal steps may negatively affect the underlying 3D perovskite and introduce time and energy inefficiencies (Jiang et al., 2021), Consequently, direct deposition without post annealing has used as a promising strategy to protect the bulk 3D perovskite while minimizing interfacial charge transport barriers. This approach not only maintains bulk integrity but also promotes defect passivation without introducing a significant resistive interface (Jiang et al., 2019).

The most efficient way to enhance the performance of PSCs devices often involves treating their surfaces, since the surface is particularly exposed to imperfections. Consequently, the application of 2D perovskite materials for surface defect treatment

become a promising approach (Cho et al., 2018; Iagher & Etgar, 2018). Due to the strong electronegativity of fluorine, fluorinated organic ammonium halides typically repel water and shows poor wettability. Poor wettablity resulted from reduced dispersion forces is the main reason for their use as passivation layers in the form of 2D perovskites to create stable and high performing PSCs (Chen et al., 2020; Ishikawa et al., 2020). Jiang, Q., et al., (Jiang et al., 2019), demonstrated that the direct application of phenethylammonium iodide (PEAI) for 3D perovskite surface passivation, without forming a distinct 2D layer, resulted in a significant PCE of 23.3%, attributed to a reduction in defect density. In contrast, Researchers led by Bolink also described the creation of 2D/3D/2D perovskite structures with well-defined boundaries by employing a dual-source vacuum deposition method (La-Placa et al., 2019). Nevertheless, the resulting PEA_2PbI_4 2D perovskite layer, which exhibited a parallel arrangement and high compositional uniformity, was found to significantly impede the movement of electrical charges. This suggests that while 2D perovskite passivation exhibit great potential, the specific processing condition, method and resulting interfacial properties are critical. Ultimately, future surface passivation strategies may also benefit from innovative approaches such as the solution based integration of perovskite quantum dots (Wu et al., 2022).

In this work we focused on surface passivation of triple cation perovskite materials, specifically $Cs_{0.05}(MA_{0.02}FA_{0.98})_{0.95}Pb(I_{0.98}Br_{0.02})_3$, using PEAI. This post deposition surface treatment strategy is designed to reduce surface defect densities and suppress nonradiative recombination, thereby enhancing the V_{oc}, FF and overall PCE. By avoiding the formation of a distinct insulating 2D layer, this approach maintains favorable charge transport pathways and demonstrates the critical role of interface-sensitive passivation strategies in boosting the performance of PSCs. Through various optical and electrical characterizations, we found that PEAI surface passivation enhances both photoluminescence (PL) and electroluminescence (EL) emission, without altering the intrinsic optical properties of the device.

1.2 Statement of problem

Nowadays PSCs become thematic research area as a promising PV technology due to their advantage such as cost effectiveness and high PCEs. despite, the advancements in PSCs development and the achievement of high PCEs, the performance of these devices is challenged by losses within the perovskite layer (Sharma et al., 2022). The formation of nonradiative recombination within the perovskite material are the critical challenge in PSC technology (Wolff et al., 2019). Specifically, nonradiative recombination occurs most of the time at surface and grain boundary sites of perovskite materials, so that the energy is lost as heat instead of being converted to electricity (Luo et al., 2020). To tackle the issue of nonradiative recombination, a different of surface passivation techniques have been developed. Among these, the utilization of organic ammonium halide salts to passivate surface and grain boundary sites has demonstrated considerable promise in reducing nonradiative recombination. This thesis investigates the use of phenylethylammonium iodide (PEAI) to passivate the surface of 3D perovskite layer without post annealing process, aiming to mitigate nonradiative recombination and thereby enhance the efficiency of PSCS.

1.3 Objectives

1.3.1 General objective

The general objective of this thesis is to improve the efficiency of PSCs ($Cs_{0.05}(MA_{0.02}FA_{0.98})_{0.95}Pb(I_{0.98}Br_{0.02})_3$) by employing phenylethylammonium iodide (PEAI) to passivate surface of perovskite layer.

1.3.2 Specific objectives

To achieve the goal of this study, the specific objectives can be summarized as below:

- To synthesis $Cs_{0.05}(MA_{0.02}FA_{0.98})_{0.95}Pb(I_{0.98}Br_{0.02})_3$ thin film by spin coating and characterize it by XRD, UV, PL, EL, and SEM.
- To passivate surface of $Cs_{0.05}(MA_{0.02}FA_{0.98})_{0.95}Pb(I_{0.98}Br_{0.02})_3$ with PEAI solution by spin coating method and characterize the PEAI treated perovskite film with XRD, UV, PL, EL, and SEM.
- To fabricate planar inverted perovskite solar cell device with sequence of glass/ITO/MeO-2PACz/$Cs_{0.05}(MA_{0.02}FA_{0.98})_{0.95}Pb(I_{0.98}Br_{0.02})_3$/(PEAI)/$C_{60}$/BCP/Cu and characterize device with J-V and EQE.

1.4 Significance of the study

To satisfy the increasing global energy demand, the pursuit of renewable and environmentally friendly energy sources has become critical. For the past 40 years, the world energy consumption has more than doubled, reaching around 18.5 terawatt-years by 2022 (Polo, 2021). Prediction indicate that, between 2020 and 2040, global energy consumption from fossil fuels such as natural gas , oil, and coal is predicted to grow at an average annual rate of 0.6% (Zhukovskiy et al., 2021). However, these conventional energy sources are become a large contributors to carbon dioxide (CO_2) emissions, which are the main factor of anthropogenic greenhouse gases and global warming. In Ethiopia, a substantial portion of the population resides in rural areas, where access to electricity remains limited to access. The nation electricity supply is basically generated from hydropower, accounting for over 96%, while biofuels continue to meet the majority of household energy needs for cooking, heating, and off grid lighting. Nevertheless, Ethiopia has set an ambitious goal to transition toward carbon neutral energy sources by 2025 (Njenga & Phiri, 2024). The development of renewable energy technologies specifically, highly efficient solar cell devices, possess a promising option to tackle global energy and environmental challenges. This work aims to contribute to better energy access for rural populations in Ethiopia by harnessing solar power. Importantly, the fabrication approach explored in this study enables the production of PSCs inside controlled environments, such as glove boxes, thereby enhance the overall efficiency of the devices.

1.5 Scope of the study

This study is centered on the preparation and characterization of PSCs that contain a mixed-cation, mixed halide perovskite absorber layer with the composition $Cs_{0.05}(MA_{0.02}FA_{0.98})_{0.95}Pb(I_{0.98}Br_{0.02})_3$. This perovskite material was synthesized by dissolving perovskite precursor in 4:1 ratio of DMF and DMSO respectively, whereas the interfacial layers MeO-2PACz and phenylethylammonium iodide (PEAI) were prepared by dissolving their precursors in ethanol and isopropanol solvents, respectively. Then the device was fabricated by spin-coating MeO-2PACz as HTL material on ITO glass, followed by annealing on hot plate, perovskite active layer were then deposited by spin coating, and subsequent coating of the PEAI passivation layer. Finally the device is transferred to chamber where thermal evaporation of C_{60} and BCP electron transport layers are take place, and finally, copper (Cu) was deposited as the top electrode, resulting in a complete p-i-n structured device with the configuration with and without PEAI treatment as ITO/MeO-2PACz /$Cs_{0.05}(MA_{0.02}FA_{0.98})_{0.95}Pb(I_{0.98}Br_{0.02})_3$/PEAI/$C_{60}$/BCP/Cu. Then once the synthesis of perovskite films were done, it is subjected to different characterization techniques including X-ray diffraction (XRD), ultraviolet-visible (UV-Vis) spectroscopy, photoluminescence (PL), electroluminescence (EL), and scanning electron microscopy (SEM) to evaluate their structural, optical, and morphological properties. Finally, the fabricated devices, with and without the PEAI passivation, were characterized for photovoltaic performance using J–V measurements under simulated solar illumination, enable to study the photovoltaic efficiency and the role of surface passivation in device performance enhancement.

CHAPTER TWO

2. LITERATURE REVIEW

2.1 Solar energy

Energy generation has become a serious issue since the industrial revolution, especially with the rapid growth of the world population. This increase the need for energy, specially electrical energy, which is fueled by the expansion of migration to previously unpopulated areas, communities, and ongoing technological progress. (Jaiswal et al., 2022). Natural gas, oil, and fossil fuels coal have been the dominant sources of energy worldwide (Deshmukh et al., 2023). Fossil fuels like oil, coal, and natural gas are nonrenewable energy sources that originate from ancient organic material (Hafezi & Alipour, 2021). They are known for their high energy density and established infrastructure, they are efficient and easy to apply (Kumar & Rathore, 2023).

The use of fossil fuels is a major source of CO_2 emissions, which drive significant climate change and environmental degradation (Andrew, 2020). Furthermore, the extraction of these resources leads to their depletion and poses various environmental hazards. Dependence on fossil fuels can also fuel geopolitical instability and economic insecurity due to fluctuating supply and prices. Consequently, the adoption of reliable, environmentally friendly, and efficient energy alternatives is crucial for ensuring a sustainable and healthy future(Almalki et al., 2023).

A range of sustainable energy options, such as solar, wind, hydropower, and geothermal power (as depicted in Figure 1), offer environmentally benign solutions that warrant serious consideration. (Amjith & Bavanish, 2022). For a number of reasons, solar energy sticks out among these as a particularly promising choice going forward. First of all, Out of renewable energy sources, solar energy is the most plentiful. The Earth absorbs roughly 1.8×10^{14} kW of the energy that the sun emits at a rate of 3.8×10^{23} kW. Heat and light are the forms that this energy comes in as, but as it passes through the atmosphere, a large portion of it is lost to cloud dispersion, reflection, and absorption. Solar energy is abundant and readily available, making it a strong contender to meet the world's energy demands even in spite of these losses (El-Afifi, 2024).

2.2 Photovoltaic technology

Photovoltaic (PV) devices, predominantly based on semiconductor materials such as silicon, generate electricity by inducing electronic excitation. The fundamental mechanism involves the absorption of incident light, which provides the energy necessary to promote electrons from lower to higher energy states. This excitation process generates a substantial concentration of mobile charge carriers within the semiconductor, ultimately leading to the production of electrical current (Rahman et al., 2022). Various photovoltaic technologies exist, including multi-junction cells, monocrystalline silicon, polycrystalline silicon, amorphous thin-film, cadmium telluride (CdTe), copper indium gallium selenium (CIGS), copper zinc tin sulfide, OSCs, dye-sensitized solar cells, and PSCs.

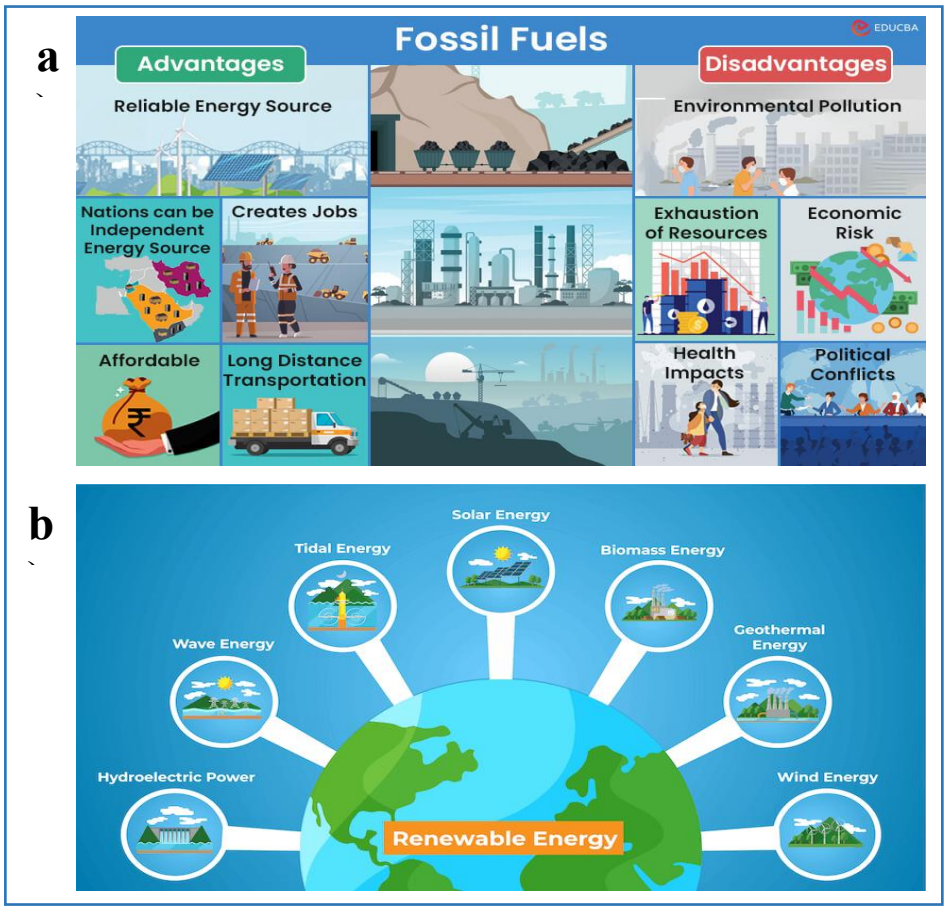

Figure 1. Fossil fuel based (a) and renewable energy source (b) (Hoppe & Sariciftci, 2004).

2.3 Perovskite structure

In 1839, Gustav Rose identified a naturally occurring mineral with the chemical composition calcium titanate ($CaTiO_3$). The term "perovskite structure" now denotes any material exhibiting the same fundamental crystal lattice arrangement as this initial discovery (Passi & Pal, 2021). Perovskite materials are characterized by the general chemical formula ABX_3, where the A-site is occupied by monovalent cations such as formamidinium (FA, $CH(NH_2)_2^+$), methylammonium (MA, $CH_3NH_3^+$), and cesium (Cs^+). The B-site is typically occupied by divalent cations, most commonly lead (Pb^{2+}) or tin (Sn^{2+}), while X represents halide anions that coordinate with both A and B cations. Within the canonical perovskite crystal structure, the B cation resides at the center of an octahedral $[BX_6]^{4-}$ unit, and the A cation is coordinated by twelve X anions in a cuboctahedral geometry. The cubic structure is generally considered the optimal perovskite configuration, as illustrated in Figure 2 (Singh, 2019).

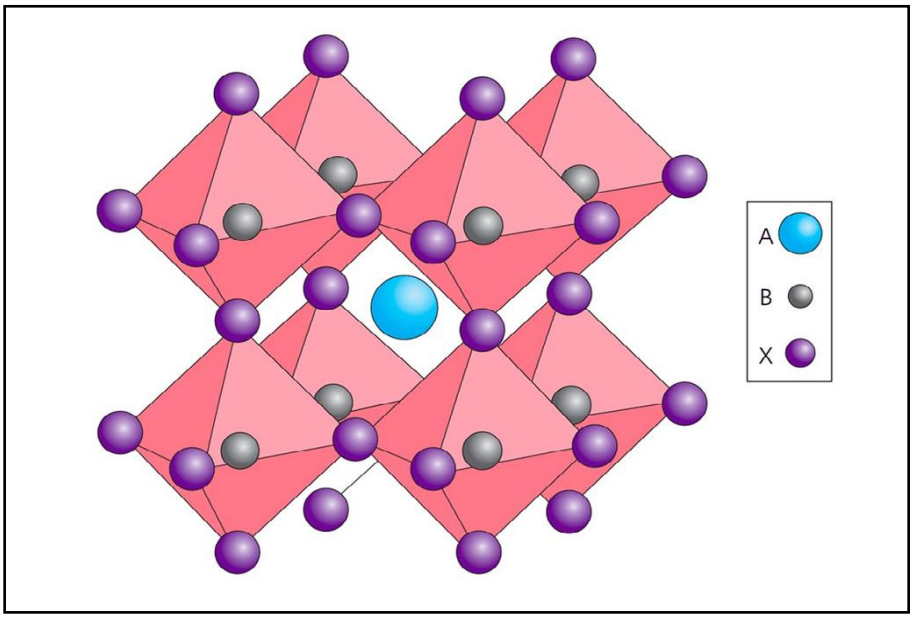

Figure 2. Perovskite crystal structure (Green et al., 2014).

The structural stability of a given perovskite can be calculated using the Goldschmidt tolerance factor (t), which is quantified using the following equation 1.

$$t = \frac{r_A + r_X}{\sqrt{2}(r_B + r_X)} \quad \text{.....(1)}$$

Where r_A, r_B and r_X stands for effective ionic radii of A, B, and X respectively.

t for perovskite materials lies in the range of 0.8-1.0. Ideally, if *t* is greater than 1 results in hexagonal or tetragonal structures and when *t* is greater than 0.9 and less than 1 it become a cubic structure, it is orthorhombic or rhombohedral structure when *t* is greater than 0.7 and below 0.9, and in case of *t* is less than 0.71 it does not produce a perovskite crystal structure figure 10. (a,b) (Mazumdar et al., 2021). Where a complete cubic system is indicated by t = 1. If t is less than 0.8, the A site cation is too small; if t is greater than 1, the A cation is too large. Both circumstances prevent formation of perovskite and could result in distinct crystal structure (Guvenc et al., 2024). Perovskite materials have many advantages. The capacity to construct a wide range of structures by altering the A, B, and X ions, as shown in Figure 3, leads to a huge family of perovskites. The capacity of these materials to tune their band gap by adjusting the A, B, and X components is a unique feature (Miah et al., 2024). Perovskites have a large dielectric constant, direct optical band gap, excellent absorption coefficients, and low exciton binding energy, and a , making them promising for a variety of optoelectronic applications such as lasers (Lei et al., 2021), light-emitting diodes (D. Yang et al., 2022), transistors (Abiram et al., 2022), and solar cells (Dey et al., 2021).

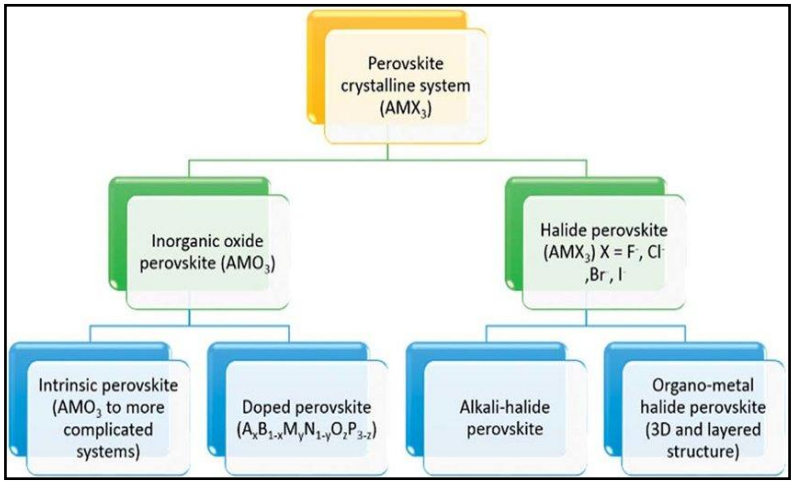

Figure 3. Perovskite crystalline system (Hettiarachchi et al., 2015).

2.4 Perovskite solar cells (PSCs)

PSCs is one of the renewable energy technologies in the past decade due to their remarkable PCE, low fabrication cost, and tunable optoelectronic properties (Yun et al., 2018). To substitute non renewable energy source such as fossil fuels, PSCs have gained attention due to their environmental friendly and affordable electricity. The first reported PSC in 2009 by Miyasaka *et al*., has PCE of just 3.8%, by using a liquid electrolyte-based structure (Tiep et al., 2016). After that, the PSCs technology shows rapid enhancement in material engineering, device architecture, and interface passivation. As a consequence of these intensive research efforts, the certified PCE of single-junction PSCs has dramatically increased to over 27% in recent years, as shown in Figure 4. High performance of PSCs is associated to their several unique properties of hybrid organic-inorganic lead halide perovskites, such as high absorption coefficients, long charge carrier diffusion lengths, low exciton binding energy (Zhou et al., 2024). These properties of PSCs enable them to efficient light harvesting and charge transport, making PSCs well-suited for both single-junction and tandem solar cell configurations.

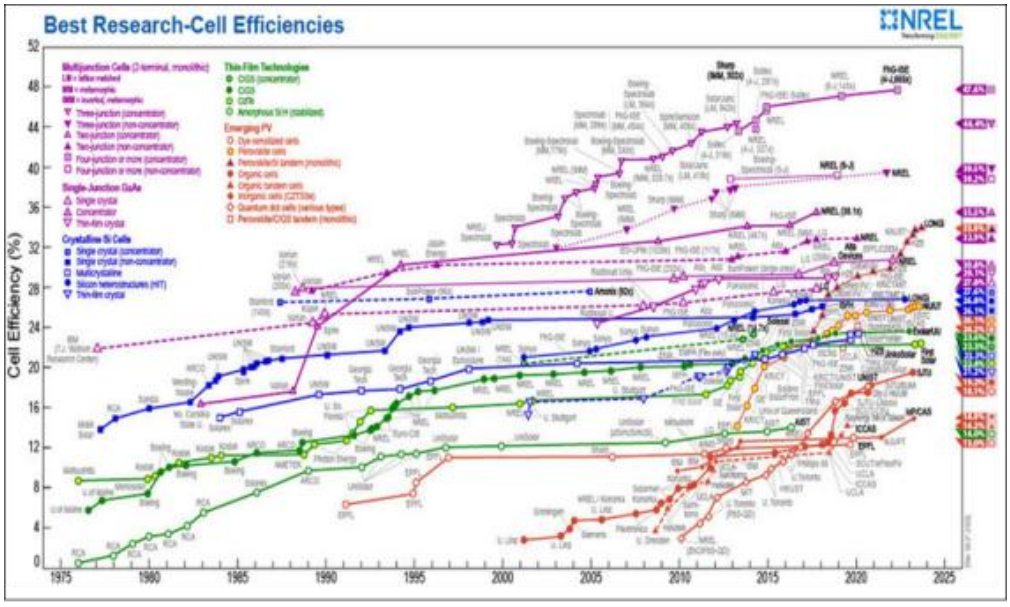

Figure 4. The solar cell efficiency trend over a years "NREL (2025)".

2.4.1 Basic working principles of perovskite solar cells

Solar cells generally work by utilizing the photovoltaic properties of semiconductor materials to convert solar energy into electricity, a process of energy conversion. The fundamental ideas behind PSCs can be summed up in four steps as shown in figure 5 either in n-i-p or p-I-n geometry of device. The light from the source stricts the perovskite active layer and the photon with suitable wavelength to the band gap of active materials is absorbed. As the result of photo absorption electron are moved to the conduction band of perovskite, by creating hole in the valency band, which are also used as charge carriers. The generated electron and hole are collected by electron transport layer (ETL) and hole transport layer (HTL) respectively. Excited and free electrons are transported from perovskite layer to the electron transport layer and arrive at the transparent conducting oxide (TCO), which can be indium tin oxide (ITO) or fluorine doped tin oxide (FTO). In parallel, hole move to the HTL and reach at metal electrode. Finally, the TCO and electrodes are connected, electrons flow through the external circuit, producing photocurrent, while electron hole recombination occurs afterward.

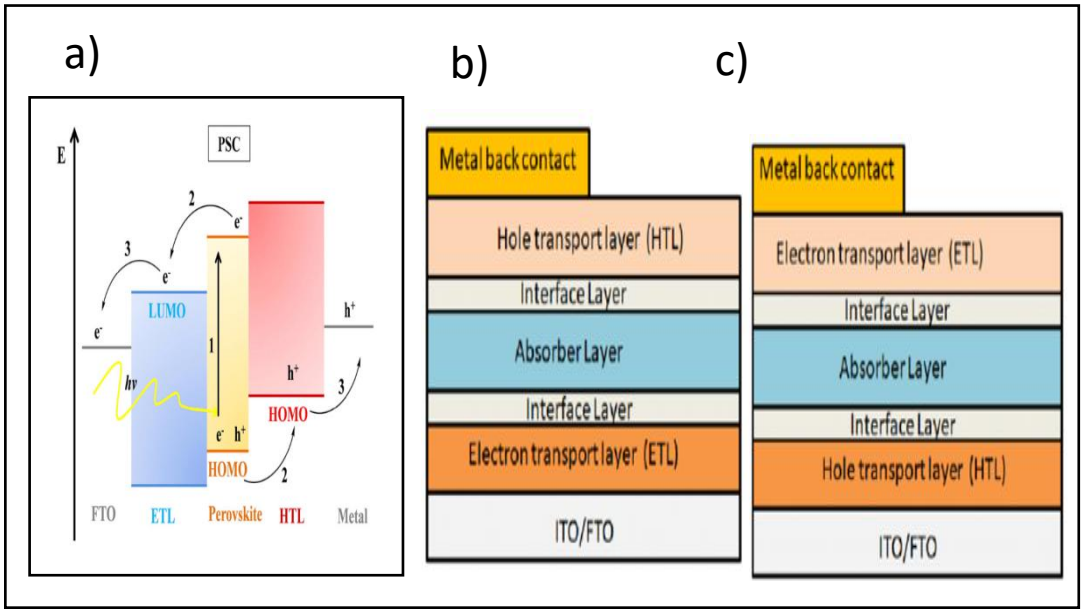

Figure 5. a) Work principles of perovskite solar cells b) n-i-p and c) p-I-n device architecture (Kheralla & Chetty, 2021).

2.5 Photovoltaic parameters

In PSCs operation condition, as a light from the source strikes the cell, there is the conversion of light energy to electrical energy. To quantify those phenomenons there are photovoltaic parameters such as Voc, Jsc, FF and PCE as shown in figure 6.

2.5.1 Short circuit current density (J_{sc})

A short circuit current can be defined as a current that flows through a solar cell when the applied voltage is zero or it is representative of the number of exciton generated and collected by their respective electrodes at zero applied potential(Fung & Choy, 2013). J_{sc} is primarily determined by the active layer material's ability to absorb light and generate excitons, which is basically determined by the material band gap and absorption coefficient, as well as the exciton diffusion across interface, which varies with the exciton diffusion lengths of the materials.

2.5.2 Open circuit voltage (V_{oc})

This is the voltage when there is no current flowing through a solar cell under light illumination or is the measure of the maximum of the voltage that a solar cell can extract for an external circuit. Because of several loss mechanisms, the photogenerated charge carrier is canceled out in this scenario (Tegegne, 2018). In conventional single junction inorganic solar cells, the Voc is governed by the band gap of the absorber materials, but it is forced by charge recombination through radiative mechanisms (Shockley & Queisser, 1961).

2.5.3 Fill factor (FF)

The fill factor is defined as the measure of the squareness of the J-V curve or the ratio of the maximum power to the product of short circuit current and open-circuit voltage which is given by the equation (2):

$$FF = \frac{V_{max} \times I_{max}}{V_{oc} \times J_{sc}} \qquad (2)$$

Where V_{max} and I_{max} are the voltage and the current at the maximum power (P_{max}) point respectively. The FF can be limited by factors such as the dependence of charge generation and extraction on the electric field. When PSCs exhibits no field dependence, the FF can potentially reach values close to 1. Additionally, imbalanced charge transport also restricts the FF (Zhou et al., 2010) i.e. different electron and hole mobility because unbalanced charge transport results in a space charge limited photocurrent which in turn limits the FF. The FF is also related to the solar cell quality and its electrical resistances.

2.5.4 Power conversion efficiency (PCE)

The ratio of a solar cell's electrical output to the input power to which it is exposed is known as solar cell power conversion efficiency. This can be calculated by dividing the maximal output power density (P_m, in W/m^2) by the incident light irradiance (P_L, in W/m^2), as follows:

$$\eta = \frac{P_{out}}{P_{in}} = \frac{FF(V_{oc}\, x\, J_{sc})}{P_{in}} \qquad (2)$$

Whereas P_{out} and P_{in} stands for the power output and input respectively.

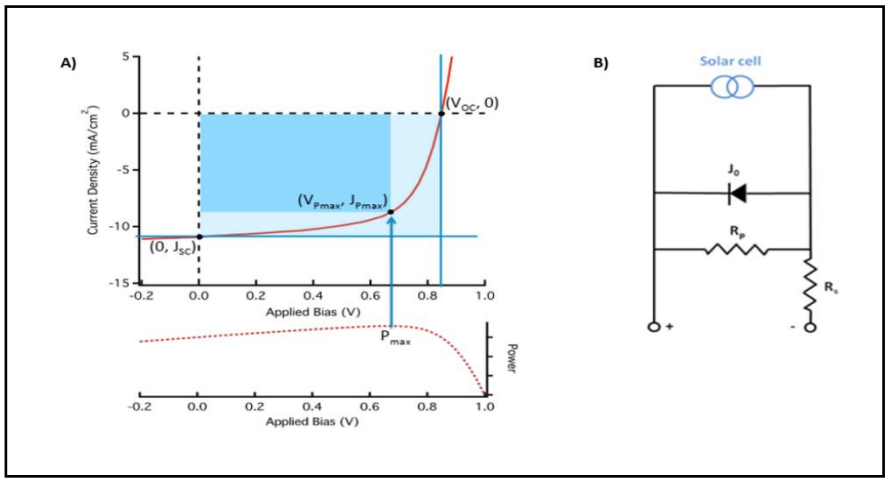

Figure 6. (a) Current-voltage (J-V) characteristics illustrating the performance of a solar cell. (b) The corresponding equivalent circuit model, where Rsh represents the shunt resistance associated with leakage currents, and RS denotes the series resistance arising from impediments to current flow within the cell (Braid, 2016; Gehrig, 2015).

2.6 Materials systems in PSCs

A solar cell device consist an absorber layer, where the generation of exciton takes place. For efficient charge transport, the active layer must be enclosed by suitable hole and electron transport layers. The device is then finalized with asymmetric electrodes. This section provides an overview of the materials commonly used as hole transport layers, electron transport layers, and absorber layers in organic-inorganic perovskite solar cells (PSCs).

In PSCs, five key components are essential for optimal device performance: a transparent conductive oxide (TCO), hole transport layer (HTL), perovskite absorber layer, electron transport layer (ETL), and a metal-based cathode (back contact) (Roy et al., 2020). Among these components, the ETL and HTL along with perovskite layer

play significant roles in PSC operation. Perovskite materials serve as the light-absorbing medium in the device, generating electron-hole pairs upon exposure to incident light. The HTL is responsible for selectively extracting holes from the perovskite absorber while simultaneously blocking the transport of electrons. It functions as a physical and energetic barrier between the perovskite layer and the ETL, effectively preventing unwanted electron transfer across the interface. (Pitchaiya et al., 2020).

2.6.1 Structural and photovoltaic properties of single-cation lead halide perovskites

Single cation perovskites is a perovskite materials that incorporate only one type of monovalent cation as A-site in their crystal structure, including methylammonium lead iodide ($MAPbI_3$), formamidinium lead iodide ($FAPbI_3$), and cesium lead iodide ($CsPbI_3$), have been foundational in the rapid evolution of PSCs (Lin et al., 2023). These materials have the general ABX_3 structure, where A is a monovalent cation (MA^+, FA^+, or Cs^+), B is divalent cation such as Pb^{2+} or Sn^+, and X is I^- (Li, 2025). The choice of A-site in perovskite structure can highly affects the structural stability of materials, optoelectronic properties, and photovoltaic performance of device (Fu et al., 2019). $MAPbI_3$ was the first perovskite materials used as best candidate for solar cell performance. $MAPbI_3$ retain a tetragonal structure at room temperature but it change to cubic phase above temperature of 54°C (Bonadio et al., 2023). The optical band gap of $MAPbI_3$ depend on the processing condition however it is known for a direct band gap with average optical band gap of 1.52 eV (Ke et al., 2015). High charge carrier mobility and high absorption capacity in visible range of light, making it highly effective for single junction devices (Jung et al., 2022). However, the organic methylammonium cation suffers from instability of device due to thermal and environmental moisture. (Ava et al., 2019) .

In this context, $FAPbI_3$ has been introduced as an alternative due to its smaller optical band gap of around 1.48 eV, which allow them to absorb high amount of visible light so that they are suitable for solar energy conversion to electrical energy as shown in figure 7 and 8 (RaeisianAsl et al., 2022). Its black phase, photoactive α-phase has a cubic perovskite structure and known for enhanced thermal stability and enhanced light absorption proprieties. However, this α-phase is not stable at room temperature

and changed into the yellow δ-phase, which is photoinactive, which limit device performance (Chen et al., 2021). With all those challenge, they show PCEs up to 25% when α-$FAPbI_3$ is stabilized using additives or compositional engineering. For instance, Chen et al.,(2021) demonstrated that adding small amounts of Cs^+ or MA^+ can effectively suppress the phase transition and stabilize the black phase of $FAPbI_3$ (Chen et al., 2021), resulting in enhanced device durability and reproducibility.

The finding for thermally stable perovskite materials led to the development of the all-inorganic $CsPbI_3$, in which the organic A-site cation is replaced with a smaller and more stable inorganic Cs^+ ion (Z. Yao et al., 2021). $CsPbI_3$ in its cubic black phase has 1.73 eV band gap, slightly better than the optimal range but still suitable for use in tandem solar cells (Ahmad et al., 2017). The key advantage of $CsPbI_3$ is its high thermal and photostability due to the absence of volatile organic components (Z. Yao et al., 2021). However, a main limitation of the $CsPbI_3$ is its instability of the cubic black phase at elevated conditions. The material tends to convert to the orthorhombic δ-phase at room temperature, which is photoinactive and lacks the desirable photovoltaic properties (H. Yao et al., 2021). A breakthrough by Swarnkar et al. (2016) showed that quantum dot synthesis and surface passivation could stabilize the cubic phase at room temperature, achieving over 10% efficiency in $CsPbI_3$ based quantum dot solar cells. Since then, a different approach have been suggested, including strain engineering, doping, and dimensional control to stabilize the black perovskite phase of $CsPbI_3$ in thin film devices (Swarnkar et al., 2016).

Despite these properties, each of these single-cation perovskites faces some problems that have push researchers toward mixed cation Techniques. However, studying these single cation systems is critical to understanding the relationships between composition, structure, and device performance of the device. Methylammonium-based perovskites serve as a baseline for device fabrication processes and defect physics (Howard et al., 2022). Formamidinium based perovskite offer insights into phase stability and band-gap tuning, while cesium based perovskites are a key for developing all-inorganic and high temperature resistant devices (Kim et al., 2025).

Recently the passivation and additive strategies tailored for each cation. For $MAPbI_3$, addition of long-chain alkylammonium ions such as phenethylammonium (PEA^+) has shown suppress of ion migration and reduce nonradiative recombination (Yi, 2021).

$FAPbI_3$ stability has been enhanced using additives like methylammonium chloride (MACl) and rubidium ions (Rb^+), but $CsPbI_3$ stabilization has benefitted from the grain boundary passivation and surface ligands such as oleic acid and oleylamine in quantum dot systems (Fan et al., 2019). Singh et al., (2019) demonstrated that combining Cs^+, FA^+, and MA^+ into a triple-cation system yields not only enhanced phase stability but also improved device reproducibility and efficiency exceeding 21% (Singh et al., 2019).

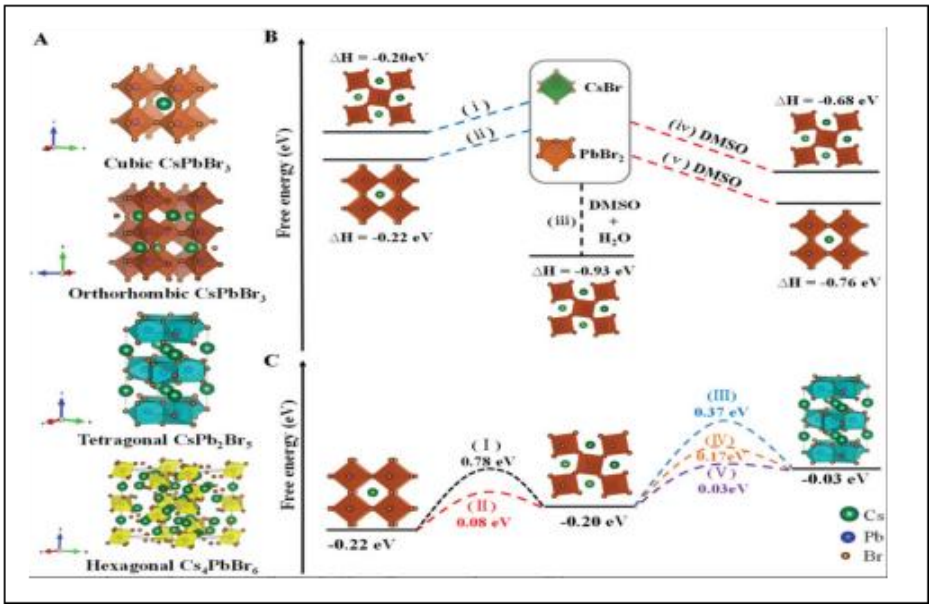

Figure 7. Crystal structure of $CsPbI_3$ (a), along with the temperature induced phase transitions that alter its structural configuration as the material transitions between different crystallographic phases (Ahmad et al., 2017; H. Yao et al., 2021).

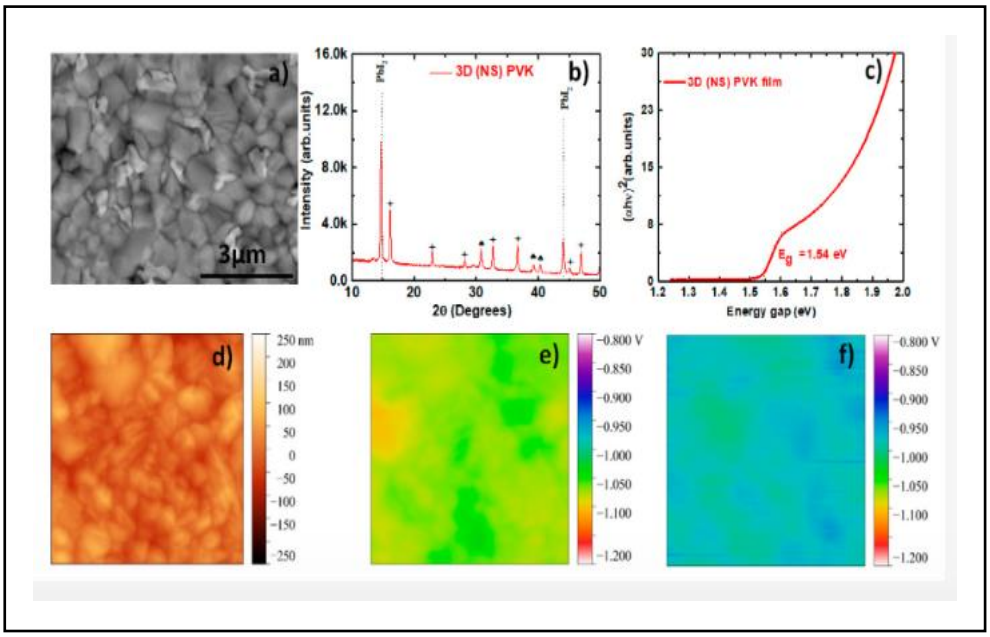

Figure 8. Surface morphology of the $FAPbI_3$ perovskite film derived from a non-stoichiometric (NS) precursor solution is presented in the SEM image (a); the corresponding X-ray diffraction (XRD) pattern of the NS perovskite is shown in (b); the optical band gap determined via Tauc's plot is illustrated in (c); three-dimensional topography of the NS perovskite active layer without octylammonium iodide (OAI), obtained using atomic force microscopy (AFM), is depicted in (d); surface potential measurements conducted by Kelvin probe force microscopy (KPFM) in the dark and under white light illumination on the same 3D NS perovskite film are shown in (e) and (f), respectively (Chung et al., 2012; Zheng et al., 2019).

To address the stability issue of single-cation perovskites, researchers began exploring mixed cation compositions, leading to the development of dual-cation perovskites. By mixing two or more second, more stable cation, such as formamidinium (FA^+) or cesium (Cs^+), into the A-site of the perovskite structure, the materials exhibited improved thermal and environmental stability (An et al., 2021). The cation mixing enable for tuning of the perovskite's electronic and optical properties, leading to higher efficiencies. The science behind mixed cations lies in their ability to reduce the structural strain within the perovskite lattice and increase the formation energy, thus making the material more resistant to degradation (B. Yang et al., 2022). Dual cation perovskites represented a significant step forward in perovskite solar cell technology.

The finding for even greater stability and performance of device has driven the development of triple cation perovskites. These materials incorporate three different cations at the A-site, typically a combination of MA^+, FA^+, and Cs^+ (Ma et al., 2024). The mixing of a third cation further enhance the stability of perovskite structure, they shows enhanced resistance to moisture, heat, and light exposure (Zhou et al., 2022). This enhanced stability is crucial for the long-term operation of perovskite solar cells in commercialization. Triple cation perovskites also known for their tunable band gap and other optoelectronic properties, enabling the fabrication of high efficiency devices with improved spectral response and reduced voltage loss (Miah et al., 2024).

Current research on PSCs is highly focused on triple cation compositions due to their superior stability and performance. Recent advancements have demonstrated remarkable PCEs exceeding 27% for triple cation perovskite solar cells, approaching the efficiencies of traditional silicon-based solar cells (Kahandal et al., 2024). Ongoing efforts are performing towards further improving the long term operational stability of these devices, reducing or eliminating the use of toxic lead, and developing scalable and cost-effective fabrication methods. The better stability and efficiency of triple cation perovskites create critical pathway towards the commercialization of perovskite solar cell technology and the realization of its full potential as a sustainable energy solution.

2.6.2 Advantages of dual and triple cation perovskites for solar cells

Now a day, PSCs have utilized as a possible alternative to conventional silicon based photovoltaics, causing a substantial fundamental change in the field of solar energy. Organic-inorganic hybrid lead halide perovskites with the ABX_3 structure have received are widely studied due to their excellent optoelectronic properties and ease solution processing conditions (Priyadarshini et al., 2023). The increment in power conversion efficiency has make them among candidate for next generation solar cell technology (Shah et al., 2023). The enhancement of the A-site cation within the perovskite lattice has been a significant method in the evolution of PSCs, improving both performance and stability (Ma et al., 2024).

The fundamental structure of ABX_3 perovskites conten a three-dimensional structure in which A monovalent cation and central B cation (divalent cation) (typically a metal ion like lead or tin) is octahedrally coordinated by six X anions (usually halides such

as iodide, bromide, or chloride) (Kour, 2023). The A-site cation can be a organic (e.g., MA^+, FA^+) or inorganic (e.g., cesium (Cs^+), rubidium (Rb^+)), which occupies a larger cubic octahedral site coordinated by twelve X anions (Vasilopoulou et al., 2023). The A-site cation is responsible in stabilizing the perovskite structure, and its size highly influences the Goldschmidt tolerance factor is dimensionless parameter that predicts the stability and formation of the perovskite phase (Wang et al., 2022). Goldschmidt tolerance factor value is obtained based on the equation 1, and usually their value is in between 0.8 and 1.0. being in this range typically indicates a stable perovskite structure (J. He et al., 2021). The A-site cation does not directly contribute to the valence and conduction band edges but its size can affect the lattice parameters, consequently affect the bandgap by changing the B-X bond lengths (Man et al., 2022). Therefore, the careful selection of A-site cations is important to tune the structural and electronic properties of perovskites for optimal solar cell performance.

$MAPbI_3$ achieve promising success on its early stage but those material suffer from instability which limit them from long term application (Zhu et al., 2023). they are highly susceptible to degradation when exposed to common environmental factors such as light, heat, and moisture. Moisture becomes a reason for hydrolysis of the perovskite materials when they are exposed it. When perovskite materials are exposed to light under ambient conditions where oxygen is present, a photo-induced chemical reactions can occur. These reactions affect the organic methylammonium (MA^+) cation, triggering its decomposition. As a result of this, volatile byproducts such as methylamine (CH_3NH_2) and hydrogen iodide (HI) are released. This degradation pathway leads to the breakdown of the perovskite structure, and leaving behind lead iodide (PbI_2) which is a yellow color, non-perovskite phase that is inactive in light absorption and severely detrimental to device performance is formed. (Kore et al., 2024). Elevated temperature accelerate these degradation and cause reduction in the materials bandgap as a result it increases charge carrier recombination. Encapsulation is widely used to prevent decomposition of $MAPbI_3$, but it does not prevent the decomposition of $MAPbI_3$ over long periods. These limitations indicate the need for strategies to enhance the stability of perovskite materials for their practical implementation in solar cell technology.

One of the main problem of single cation perovskite is the instability challenges associated with it. In order to solve this problem researchers come up with idea of usinging multiple cations at A site. A common approach involves combining FA with MA or Cs (Gutierrez-Partida et al., 2021). Optical bandgap of $FAPbI_3$ is more optimal for solar energy absorption compared to $MAPbI_3$ (RaeisianAsl et al., 2022). The insertion MA or Cs into $FAPbI_3$ enhance the stability and the overall PCEs (Lin et al., 2023). The goal of using mixed cations lies in achieving a more optimized material properties that are not attainable with a single A-site cation.

Stability of dual cation perovskite materials after introduction of small sizes cation is enhanced. The multiple A-site cations that occupy the A site with different ionic radii reduce the lattice strain of the perovskite structure so it leads to greater tolerance to phase segregation by optimizing the Goldschmidt tolerance factor (Wang et al., 2023; B. Yang et al., 2022). Additionally, dual-cation systems often result in the formation of perovskite films with improved morphology, characterized by larger grain sizes and fewer pinholes (Xie et al., 2023). These denser, more uniform films reduce the pathways for moisture and oxygen to penetrate the perovskite layer, thereby mitigating degradation. The initial success of mixed MA/FA cation perovskites, which showed improved efficiency due to better film quality, highlighted the potential of this approach.

For even better performance in PSCs the incorporation of different A-cite cation such as FA/MA/Cs take place which lead to the formation of triple cation PSCs. The substitution of A-site cation with three different size cation provides an additional degree of freedom for fine-tuning the structural and electronic properties of the perovskite material, often resulting in even greater enhancements in both stability and efficiency compared to dual-cation systems (Devasia, 2023). For instance, the inclusion of a small inorganic cation like cesium within the FA/MA perovskite framework can further stabilize the perovskite lattice and improve its resistance to environmental stressors(Ašmontas et al., 2021).

The synergistic effects observed in triple-cation perovskites arise from the unique contributions of each cation to the overall material properties. The different sizes and charges of the incorporated cations work together to improve film quality, reduce defect density, and optimize the bandgap (Grandhi et al., 2024). Smaller inorganic

cations like Cs can occupy interstitial sites within the lattice, potentially reducing ionic migration pathways and improving stability against heat and electric fields (Li et al., 2022). Larger organic cations like FA contribute to a more favorable bandgap for light absorption. The combination of these cations can lead to the formation of smoother, more crystalline films with fewer surface defects, which in turn enhances charge carrier transport and reduces recombination losses, ultimately boosting device performance (RaeisianAsl et al., 2022). The ability to precisely control the bandgap through the careful mixing of different A-site cations allows for the creation of perovskite materials that can more efficiently absorb a broader range of the solar spectrum.

It is demonstrated that the dual and triple cation PSCs is superior to single cation PSCs interms of stability and performance. For example $MA_xFA_{1-x}PbI_3$, achieved a higher power conversion efficiency of 14.9% compared to single-cation systems at the time, attributed to improved film quality. A stacked $FAPbI_3/MAPbI_3$ film further increase the efficiency to 16.01%. More recent studies have shown even more significant improvements. A quadruple cation device ($Cs_{0.07}Rb_{0.03}FA_{0.77}MA_{0.13}PbI_{2.8}Br_{0.2}$) achieved a high power conversion efficiency of 21.7%, but a triple cation device ($Cs_{0.1}FA_{0.6}MA_{0.3}PbI_{2.8}Br_{0.2}$) with a slightly lower PCE of 21.2% exhibited considerably better stability, resulting in about 30% more energy harvested over its lifetime (Dipta et al., 2024). This highlights a critical trade-off between peak efficiency and long-term stability, where triple cation systems often strike a better balance for practical applications. While monocation perovskites have shown better performance in HTL free solar cells, mixed cation perovskites generally perform better in standard n-i-p and p-i-n architectures, which are more commonly used. Furthermore, planar perovskite solar cells based on $FAPbI_3$, a key component in many dual and triple cation systems, have demonstrated higher photoelectric conversion efficiency compared to $MAPbI_3$ based devices .

2.7 Electron transport materials (ETMs)

In n-i-p PSC devices, where light absorption occurs in the intrinsic perovskite layer after passing through the n-type ETL, and the efficiency of operation depend on the properties of ETL. The function of the ETL is to selectively extract photogenerated

electrons from the perovskite layer and transport them towards the cathode, at the same time they effectively block the flow of holes towards the same electrode.

For a material to be a good an ETL, several key criteria must be met. Firstly, the energy level alignment between the ETL and the perovskite absorber is required (Hossain et al., 2023). Specifically, the ETL's lowest unoccupied molecular orbital (LUMO) energy level should be slightly below that of the perovskite's conduction band minimum (CBM) to help efficient electron injection. The HOMO energy level of ETLs should be significantly below the perovskite VBM to effectively block hole transport (Ahmed et al., 2020). The adjustable properties of perovskite materials, achieved through compositional engineering (e.g., by varying the A, B, and X site ions), which allow control over their energy band positions. This tunability is the cause for both an opportunity and a challenge for ETL selection. It can enable a closer energy level match with a chosen ETL and it also give the way for careful consideration of the specific perovskite composition to ensure optimal alignment for efficient charge transfer. Secondly, the ETL materials must exhibit high transmittance across a broad range of the UV-Vis spectrum. This high transparency allow light to pass through and a maximum number of photons to generate with sufficient energy to reach the perovskite absorber layer, where light absorption and charge generation take place (Bulowski et al., 2024). Any significant absorption within the ETL itself would lead to energ losses and reduced device efficiency. Thirdly, the surface morphology of the ETL plays a important role in the subsequent growth and quality of the perovskite crystal film deposited on top (Wang et al., 2021). A uniform, pinhole-free ETL surface with appropriate grain size and surface energy can enhance the formation of a high quality perovskite layer with fewer defects, so it leading to enhanced charge transport and reduced recombination. As a result, given the tunability of perovskite energy levels and careful selection of the ETL with consideration for the specific perovskite composition is important to fabricate high efficiency devices.

Different materials have been explored as ETLs in perovskite solar cells as shown in Figure 9 (a). including metal oxides such as TiO_2, SnO_2, and ZnO, as well as fullerene derivatives like PCBM (Cao et al., 2020). These materials are chosen based on their ability to extract electrons from the perovskite absorber and transport them towards the cathode. Wide-bandgap metal oxides that are commonly used as ETL, such as

TiO_2 and SnO_2, have high transmittance, so they allow more light to reach the perovskite layer. SnO_2 exhibits high electron mobility and rapid charge transport (Chen et al., 2019). C60 based materials are known for their good electron mobility and energy-level alignment.

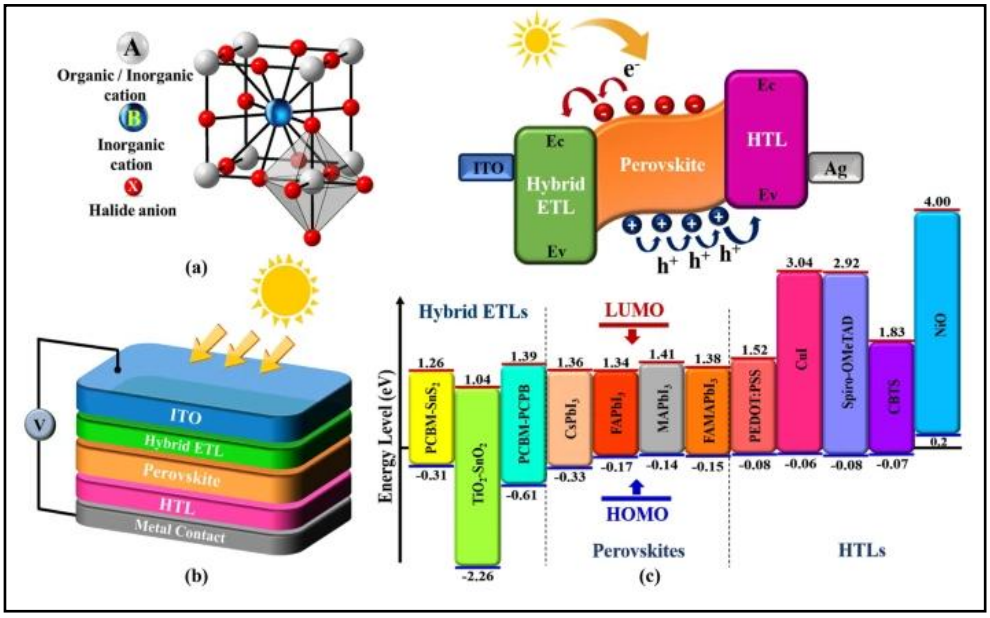

Figure 9. a) 3D cubic crystal structure representing the ideal perovskite with the general formula ABX_3; (b) a schematic layout of the inverted perovskite solar cell architecture comprising ITO/hybrid electron transport layer (ETL)/perovskite/hole transport layer (HTL)/metal electrode; and (c) a conceptual illustration of charge carrier dynamics along with a simplified flat-band energy level diagram of the perovskite solar cell as modeled and analyzed in this study (Lin et al., 2020; Subudhi & Punetha, 2023).

2.8 Hole transport materials in PSCs

Hole transport materials (HTMs) are very important for efficient PSCs as shown in figure 9 b, they transport photogenerated holes and block electrons to minimize energy loss. Proper energy level alignment of the HTM's HOMO with the perovskite absorber's valence band ensures effective hole transfer, while a sufficiently low LUMO prevents electron leakage. The HTMs is basic component in various perovskite absorber layers, including those with single, dual, and triple cation

compositions at the A-site. The energy levels (VB and CB) of the perovskite absorber can shift depending on the specific combination of A site cations. Therefore, the HTM must be carefully chosen to ensure optimal energy level alignment with the particular perovskite absorber being used, regardless of the number of different cations present at the A-site.

MeO-2PACz is self assembled monolayer classified as carbazole HTL materials, investigation for its potential to enhance PSCs performance with these different perovskite compositions. In single cation absorbers of PSCs, the HOMO level of HTMs are well align with this absorber layer, which enhance the hole extraction from the active layer (Jiang et al., 2024). For perovskite absorbers with dual and triple cation compositions, the suitability of MeO-2PACz depends on the resulting energy band positions. Researchers need to evaluate and modify the HTM or its interface to achieve optimal energy level matching and efficient charge transport for perovskite materials. Therefore, careful selection and engineering of HTMs, are very important for achieving highly efficient and stable perovskite solar cells, with respect to A-site cation composition (single, dual, or triple), by ensuring optimal energy level alignment and efficient charge transport.

Besides it energy level alignment a good HTM needs to have three major requirements that includes high hole mobility, good solubility and film-forming properties, and low cost (Ansari et al., 2018). HTL can be classified as organic, inorganic, and carbonaceous. The organic-based HTL includes long-chain polymer and small molecules, which are nearly polymeric-based. The inorganic HTL includes Nickel-based, copper-based, *p*-type semiconductor and transition metal HTMs (Pitchaiya et al., 2020). Figure 10 shows the flow chart about the classification of the HTMs.

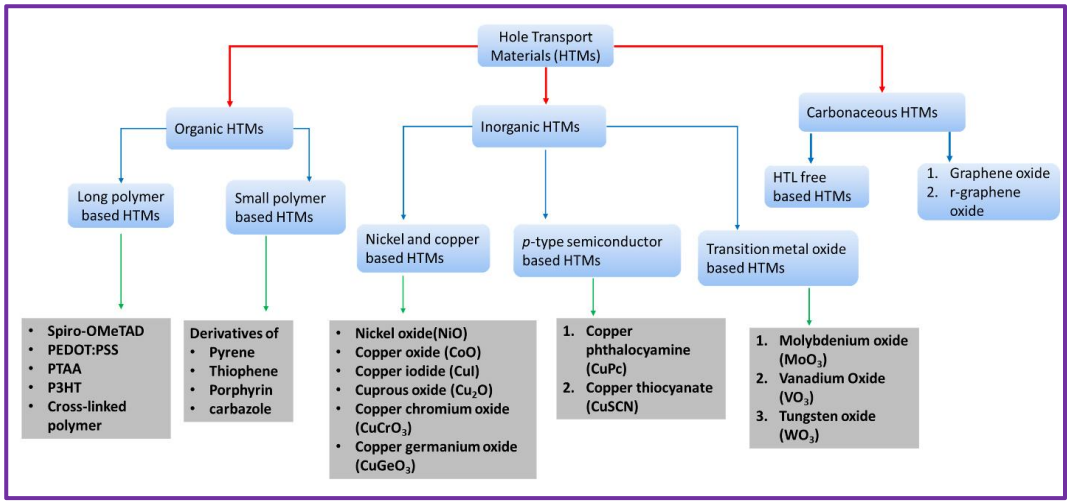

Figure 10. Flowchart illustrating the classification of hole-transporting materials (HTMs) (Pitchaiya et al., 2020).

2.9 Challenges in perovskite solar cells

Perovskite solar cell possess advantages like high efficiency, flexibility, low cost and lightweight however they still face some challenges that need to be addressed for long term commercialization of PSCs. One of the primary concern is their instability. Perovskites are highly sensitive to air, moisture, heat, and light. Currently, The most stable PSC is believed to have a one-year lifetime, while silicon solar cells have an average lifetime of more than 25 years (Grancini et al., 2017). hysterisis phenomena is also another challenge that detected when the J-V measurement of device is taken.

2.9.1 Stability

Stability problem of perovskite solar cell can be caused from both internal instability of perovskite and external factors related to ambient condition as shown in figure 11. Extrinsic instability primarly caused by external factors that are unavoidable in case of real application such as oxygen and humidity, while intrinsic instability mostly caused by molecular and crystallographic structure of the perovskite may lead to the degradation of PSCs as shown in figure 13 (Mazumdar et al., 2021).

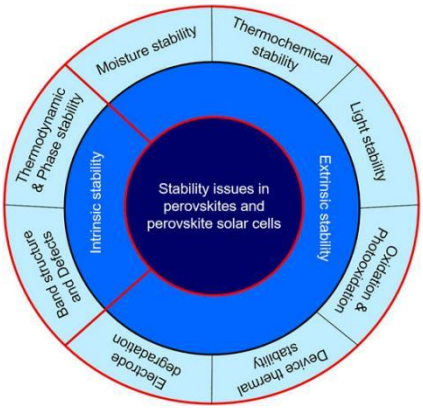

Figure 11. Source of instability in perovskite materials and perovskite solar cells (Mazumdar et al., 2021).

Moisture causes chemical processes to disrupt the hydrogen bonds in the perovskite structure, resulting in the creation of hydrated chemicals that degrade the material. Numerous studies indicate that water serves as a stimulant for this irreversible breakdown process. Figure 12. Depicts the suggested degradation mechanism for $CH_3NH_3PbI_3$ ($MAPbI_3$) perovskite, as well as the chemical events involved. While these processes are reversible under some conditions, once the perovskite is saturated with moisture, they become irreversible, and $MAPbI_3$ degrades into MAI and PbI_2.
Different ways have been suggested to improve the PSCs moisture resistance, including using a hole transport layer (HTL) to prevent moisture, adding a thin blocking layer between the perovskite and HTL, and using anti-water carbon electrodes (Asghar et al., 2017).

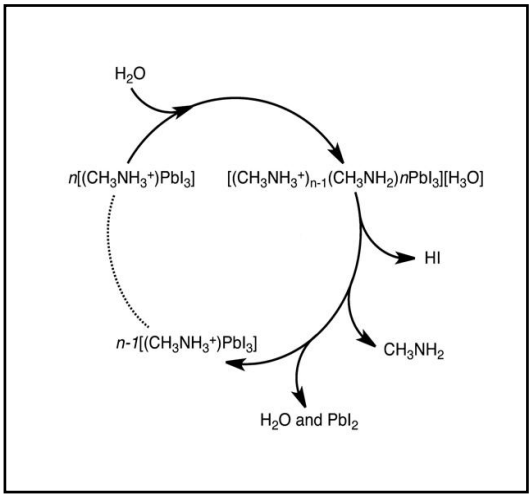

Figure 12. Moisture-induced degradation of $MAPbI_3$ perovskite (Frost et al., 2014).

Oxygen in the atmosphere can react with MA^+, Pb^+, and I^- ions in perovskite structures, forming electronic traps and charge barriers. Additionally, oxygen molecules can form Pb-O bonds on the film surface, leading to deterioration of PSCs. Encapsulating PSCs reduces the negative impact of oxygen and moisture (Duan & Uddin, 2022).

One of the most common factors influencing perovskites is water both in presence of oxygen and otherwise. Water and other polar solvents can damage perovskite because of their tendency to produce solvated phases. Polar solvents can be avoided by optimizing deposition techniques, but exposure to ambient moisture is unavoidable. Water molecules can hydrate the perovskite, forming a monohydrate phase (Askar et al., 2017).

$CH_3NH_3PbI_3(s) + H_2O(g) \rightleftharpoons CH_3NH_3PbI_3 \cdot H_2O$ …….…… (1)

$CH_3NH_3PbI_3 \cdot H2O \rightleftharpoons (CH3NH_3)_4PbI_6 \cdot 2H_2O + 3PbI_2 + 2H_2O$…….. (2)

Both reactions are reversible. So, if the hydrated products are stored in an inert or moisture-free environment, they can be dehydrated to create back perovskite with only minor irreversibility due to phase segregation. Hydration of the perovskite results in structural deformation of $(PbI_6)^{4-}$ octahedra, converting the 3D network into a 1D chain for monohydrates and 0D for dihydrates. These weaken the chemical connections between the A-site moiety and the $(PbI_6)^{4-}$, making the perovskite more susceptible to external influences like heat and electric bias. Once the perovskite is saturated with moisture, its hydration becomes irreversible, and it irreversibly decomposes to create CH_3NH_3I and PbI_2 (Christians et al., 2015).

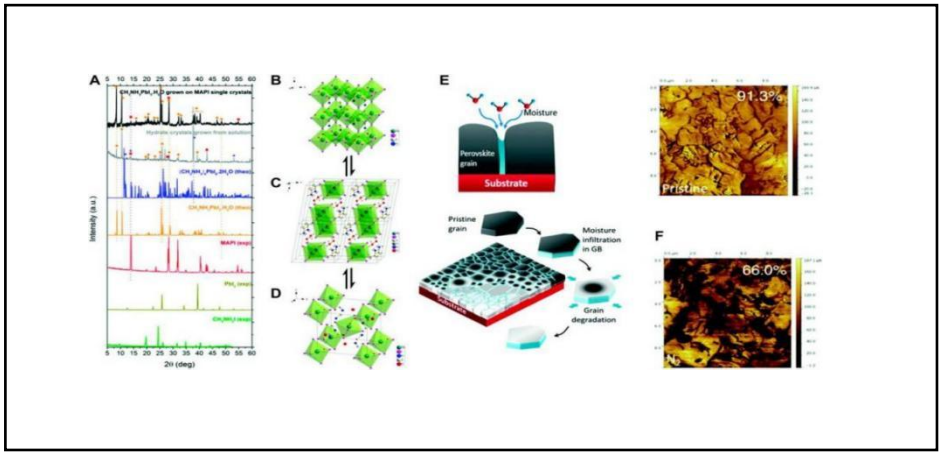

Figure 13. Intrinsic stability of perovskites. (A) Illustration of the tolerance factor (t) as a function of the effective ionic radius, indicating the likelihood of different

structural phases (X. Li et al., 2016). (B) technique of mixing of A-site species (Mazumdar et al., 2021). (C) and (D) Defect tolerance of $MAPbI_3$ as predicted by density functional theory (DFT) calculations (Mazumdar et al., 2021). (C) formation energies in three different conditions, from left to right-I-rich/Pb-poor, neutral and Pb-rich/I-poor. (D) Transition energy levels for intrinsic acceptor (left) and donor (right) point defects. (E) Correlation between the valence band maximum and the I/Pb ratio in $MAPbI_3$ films, as determined by X-ray photoelectron spectroscopy (XPS**)** (Steirer et al.).

2.9.2 Hysteresis

PSCs current density-voltage (J-V) responses can show unusual dependency on direction of scan and how fast the scan is, known as hysteresis. it can also expressed as PCE variation between scans direction when the J-V measurement take place. In general, forward scans have lower PCE than reverse scans (C. Li et al., 2016). Possible reasons of hysteresis include ferroelectric polarization, charge traps at interface, slow transient capacitive current, and grain boundaries, and ion migration (Chen et al., 2016). Ferroelectric polarization is significantly faster than hysteresis process. Trapping and detrapping processes at interfaces and grain boundaries are unlikely to be the primary cause of hysteresis due to their extended duration and significant current degradation. Ion migration theory receives greater attention than other factors (Zhao et al., 2021). Ion migration occurs when iodide (I^-) ions in perovskite travel towards ETL or HTL interfaces under varying voltage biases. This movement creates vacancies at the interfaces, causing energy band bending in the perovskite layer and between the two interfaces. Varying the energy barrier causes variations in V_{OC} and PCE values under different voltage biases, resulting in a hysteresis effect in J-V measurements (Calado et al., 2016).

The hysteresis index (HI) of a solar cell is commonly presented and can be calculated using the formula in equation 3 below. An ideal cell should have a minimum HI value.

$$HI = \frac{PCE_{reverse} - PCE_{forward}}{PCE_{reverse}} \quad \text{..... (3)}$$

2.10 Interface engineering

In PSCs, inherent imperfections and issues with exciton transport at the interface lead to charge buildup and recombination. Carrier recombination occurring within the bulk, at the ETL/perovskite interface, or at the perovskite/HTL interface leads to a reduction in VOC and FF, bringing them to values significantly below their theoretical maximums (Pan et al., 2021). Figure 14, illustrates the three primary recombination processes in PSCs: Shockley-Read-Hall (SRH) recombination, radiation recombination, and Auger recombination (Kim et al., 2020).

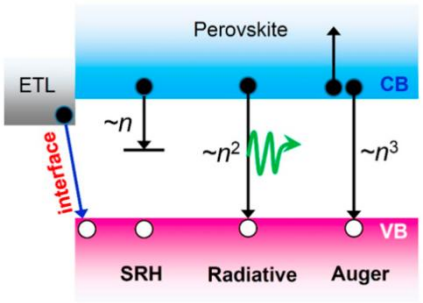

Figure 14. The PSCs recombination processes (Kim et al., 2020).

V_{OC} and FF can achieve their theoretical maximum when only radiative recombination is present, but decline when nonradiative recombination (SRH and Auger) is present (Al-Mousoi et al., 2023). Under 1 sun illumination, Auger recombination has a negligible effect on PSCs. The primary cause of nonradiative recombination loss in PSCs is SRH recombination, which is influenced by the depth of energy levels and the density of defects (Adhikari et al., 2025).

2.11 Surface Passivation

Surface passivation has emerged as a vital strategy to enhance the efficiency and operational stability of PSCs by minimizing nonradiative recombination losses and reducing surface defect states (Tao et al., 2025). Among the various passivation materials, PEAI has shown particular promise due to its ability to form a low-dimensional Ruddlesden–Popper perovskite layer on the surface of three-dimensional perovskite films (Teale et al., 2024). This quasi-2D layer effectively passivates under-coordinated ions at grain boundaries and interfaces while providing hydrophobic protection. Several studies have demonstrated the efficacy of PEAI in boosting device performance. Principe et al. (2021) reported that applying a PEAI treatment to FA-Cs-MA perovskite films increased the open-circuit voltage from 1.09 V to 1.15 V and raised the PCE from 20.3% to 22.1% due to reduced surface recombination (Principe et al., 2022). Similarly, Tong et al. (2020) observed that PEAI-treated PSCs exhibited longer photoluminescence lifetimes and superior operational stability, maintaining over 90% of their initial efficiency after 1000 hours of continuous illumination (Tong et al., 2022). Huang et al. (2022) further demonstrated that PEAI imparted significant moisture resistance, with devices retaining over 85% of their original performance under 85% relative humidity for 500 hours. In addition to PEAI, other materials have been explored for surface passivation (Huang et al., 2024). Wu et al. (2020) utilized guanidinium iodide (GAI) to form hydrogen bonds with iodide vacancies, enabling efficiencies above 23% and improved phase stability (Wu et al., 2023). Kim et al. (2019) employed methylammonium chloride (MACl) as a post-treatment to heal halide vacancies, leading to enhanced grain morphology and PCEs around 21.5%. More recently, Li et al. (2024) introduced a dual-passivation strategy by combining PEAI with fullerene derivatives (PCBM), which synergistically reduced surface and bulk trap densities, achieving efficiencies over 23.5% and improved thermal stability (Li et al., 2024). Collectively, these findings underscore that PEAI remains one of the most effective and versatile surface passivation agents, offering a combination of optoelectronic enhancement and environmental protection. Continued development of hybrid or co-passivation approaches that integrate PEAI with other functional materials holds significant promise for pushing perovskite solar cell performance closer to commercial viability.

Table 1. S*ummary of device geometries and performance of triple cation based perovskite solar cells*

No	Device geomerty	Surface treatment	**Voc (V)**	**Jsc (mA/cm²)**	**FF (%)**	**PCE (%)**	Reference
1	ITO/SnO_2/Perovskite/Spiro-OMeTAD/Au	None	1.13	22.7	82	21.1	(Ašmontas et al., 2021)
2	FTO/c-TiO_2/m-TiO_2/Perovskite/Spiro-OMeTAD/Au	Perovskite QDs	1.10	22.5	82	21.0	(Yang et al., 2020)
3	ITO/SnO_2/Perovskite/Spiro-OMeTAD/Au	CH_3O-PEAI	1.19	24.43	80.3	23.42	(Luan et al., 2021)
4	FTO/c-TiO_2/m-TiO_2/Perovskite/Spiro-OMeTAD/Au	F-PEAI	1.18	Not specified	85	23.7	(Degani et al., 2021)
5	FTO/c-TiO_2/m-TiO_2/Perovskite/Spiro-OMeTAD/Au	PEAI	1.09	22.52	78.3	19.22	(Tien et al., 2022)
6	ITO/SnO_2/Perovskite/Spiro-OMeTAD/Au	Organic Halide	1.10	22.0	80	21.0	(Zhou et al., 2019)
7	ITO/NiO_x/Perovskite/PCBM/Ag	PEAI (1.67%)	0.95	Not specified	Not specified	14.85	(Gong et al., 2021)
9	FTO/c-TiO_2/m-TiO_2/Perovskite/Spiro-OMeTAD/Au	None	1.10	22.0	80	21.7	(Dipta et al., 2024)
10	ITO/SnO_2/Perovskite/Spiro-OMeTAD/Au	GDY	1.19	24.43	80.3	23.42	(Wang et al., 2019)
11	ITO/SnO_2/Perovskite/Spiro-OMeTAD/Au	APTMS	1.09	22.52	78.3	18.03	(Shi et al., 2022)
12	FTO/TiO_2/Perovskite/HTM/Ag	None	1.16	Not specified	85	18.7	(Siegrist et al., 2021)
13	FTO/TiO_2/Perovskite/Spiro-OMeTAD/Au	PbS quantum dots	1.10	22.0	80	11.3	(Albaladejo-Siguan et al., 2019)
14	ITO/SnO_2/Perovskite/Spiro-OMeTAD/Au	DAP	1.15	Not specified	Not specified	25.29	(Taddei et al., 2024)
15	ITO/MeO-2PACz/perovskite/C60/BCP/Au	PEAI	1.15	24.4	71.9	20.6	this work

CHAPTER THREE

3. EXPERMENTAL METHODOLOGY

3.1 Materials and Chemicals

3.1.1 Chemicals

In this thesis, the following chemical precursors are utilized: Formamidinium Iodide (CH_5IN_2), Methylammonium Bromide (CH_3NH_3Br), Methylammonium Chloride (CH_3NH_3Cl), Lead Iodide (PbI_2), Cesium Iodide (CsI), N,N-Dimethylformamide $(CH_3)_2NC(O)H$), Dimethyl Sulfoxide $(CH_3)_2SO$), distilled water, ethanol, acetone, isopropanol, chlorobenzene, phenethylammonium iodide (PEAI), MeO-2PACz, fullerene(C_{60}), Bathocuproine (BCP) and Cu.

3.1.2 Materials

The list of materials that utilized in this work are ITO substrates, aluminum electrodes, micropipettes, aluminum foil, beakers, spin coater, magnetic stirrers, drying ovens, hot plates, thermal evaporators, UV Ozone cleaners, and solar simulators.

3.2 Preparation of perovskite solution and thin film

Preparation of triple cation perovskite solution ($Cs_{0.05(}MA_{0.02}FA_{0.98})_{0.95}Pb(I_{0.98}Br_{0.02})_3$) perovskite solutions of 1.73M were based on the procedure reported by (Seid et al., 2024). Typically, a FAI (277 mg), PbI_2 (909 mg including excess) MABr (3.68 mg), MACl (18.10 mg), and CsI (22.5 mg) precursors were mixed in a DMF:DMSO solvent mixture (4/1 v/v) and stirred at 60ºC for 4 hours. Then ITO glass substrates were washed with soap and thoroughly cleaned using sequential ultrasonic treatments with distilled water, ethanol, acetone, and isopropanol for 10 minutes each. Cleaned ITO substrates were UV ozone treated for 20 minutes prior to HTL/triple cation perovskite film deposition. To form the perovskite layer, the triple-cation solution was spin coated onto the substrate at 4000 revolutions per minute for 40 seconds. At 12 s before the end of spin-coating, 300 μL of chlorobenzene was dropped onto the spinning substrate as an antisolvent, and then annealed at 100 °C for 1 h.

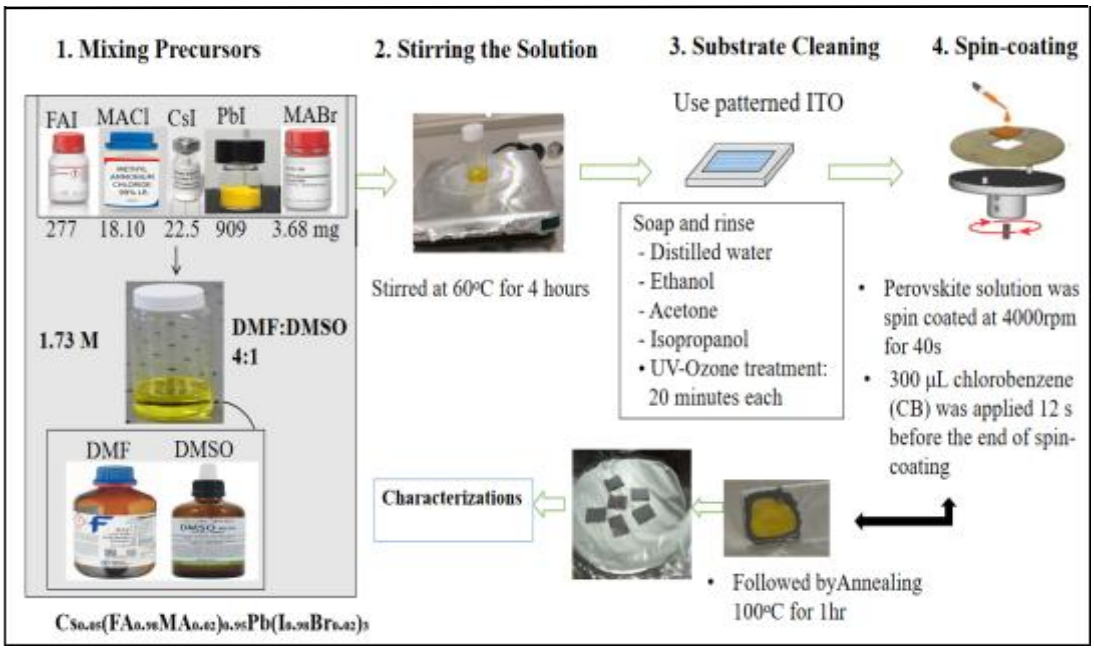

Figure 15. Preparation procedure of Triple cation perovskite solution and film

3.3 Preparation of PEAI solution

The PEAI solutions were prepared by dissolving 4.98mg of phenethylammonium iodide (PEAI) in 1ml of isopropanol to form concentration of 20mM solution. the solution were stirred for 60 minutes to ensure complete dissolution and optimal conditions for PEAI solution formation.

3.4 Surface passivation of triple cation perovskite

After preparing both triple cation perovskite solution and PEAI solution, the surface of triple cation perovskite were treated. The patterned ITO glass substrates were washed with soap and thoroughly cleaned using sequential ultrasonic treatments with distilled water, ethanol, acetone, and isopropanol for 20 minutes each. The cleaned ITO glass substrates were then be treated with a UV-ozone cleaner for 20 minutes. Then the triple-cation perovskite solution was deposited by spin-coating at 4000 rpm for 40 s. 7 s before the end of spin-coating, 300 µL chlorobenzene as antisolvent was dispensed onto the spinning substrate, followed by annealing at 100 °C for 1 h. Then, solution of PEAI were spin-coated on the cooled substrate at 5000 rpm for 40 s.

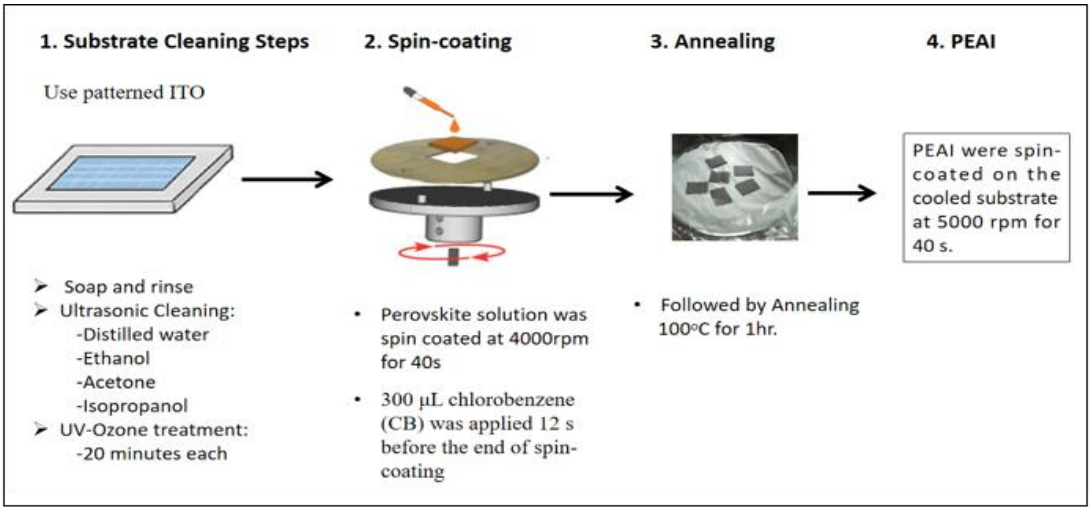

Figure 16. Surface passivation of triple cation perovskite film

3.5 Preparation of MeO-2PACz solution

1mmol/ml of MeO-2PACz solution was prepared in ethanol. To prepare a 1 mmol solution of MeO-2PACz in ethanol 1mg of MeO-2PACz measured and dissolved in 1ml of ethanol at room temperature until it become homogeneous solution.

3.6 Device fabrication

Inverted planar n-i-p perovskite solar cells were prepared with the layer sequence of glass/ITO/MeO-2PACz/$Cs_{0.05}(FA_{0.98}MA_{0.02})_{0.95}Pb(I_{0.98}Br_{0.02})_3$/PEAI/$C_{60}$/BCP/Cu as summarized in figure 17. Initially, the glass substrates were cleaned by soap and subjected to ultrasonic baths in distilled water, ethanol, acetone, and isopropanol, each for 10 minutes. The cleaned ITO glass substrates were then exposed to UV ozone treatment for 20 minutes to enhance surface preparation before depositing the MeO-2PACz layer. A 1 mmol mL^{-1} solution of MeO-2PACz was applied via spin coating at 3000 rpm for 30 seconds, then followed by thermal annealing at 100 °C for 10 minutes. Once cooled to room temperature, the triple cation perovskite layer was deposited through spin coating at 4000 rpm for 40 seconds. Twelve seconds prior to the end of spin coating, 300 µL of chlorobenzene was spin coated onto the rotating substrate as an antisolvent, and the film was subsequently annealed at 100 °C for 1 hour. For surface passivation, a 20 mM PEAI solution was spin coated onto the cooled perovskite film at 5000 rpm for 40 seconds. The films were then loaded in a vacuum evaporation chamber, where deposition of 30 nm C_{60} (at 0.3 Å/s), 8 nm BCP (at 0.3 Å/s), and 100 nm Cu (at 0.6 Å/s) was performed under a high vacuum of 10^{-7} mbar. Following evaporation, the fabricated solar cells were allowed to cool naturally to room temperature prior to characterization.

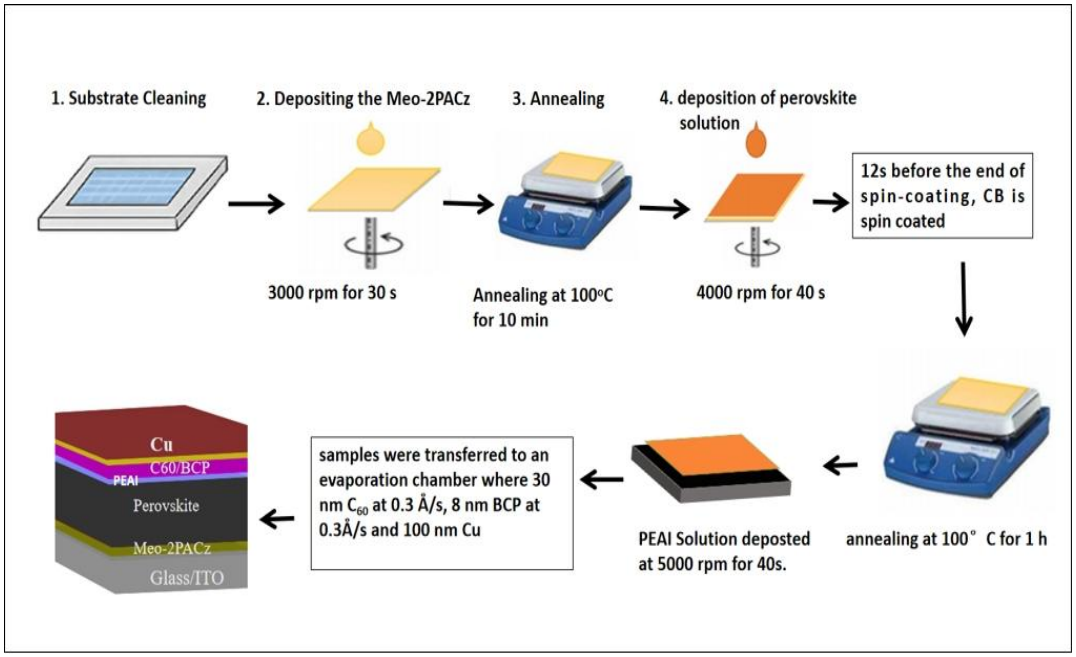

Figure 17. Device fabrication procedure

3.7 Material characterizations

The crystal structure of the fabricated perovskite thin films was examined using X-ray diffraction with Cu Kα radiation (λ = 1.5418 Å), operated at 40 kV and 30 mA, with a scan speed of 3°/min over a 2θ range of 10–60°. Optical absorption and photoluminescence (PL) spectra of the films deposited on glass substrates were recorded using a PerkinElmer Lambda 19 UV-Vis/NIR spectrophotometer and a HORIBA FLUOROMAX-4 spectrofluorometer, respectively. External quantum efficiency (EQE) measurements were performed using a custom-built small-spot EQE system, scanning wavelengths from 300 nm to 1000 nm in 5 nm steps. The light beam, measuring 2 × 5 mm², was smaller than the device's active area (~0.06 cm²). Current–voltage (J–V) characteristics of the solar cells were measured at room temperature inside a nitrogen-filled glove box using a Keithley 2400 source meter. Illumination was provided by a class AAA Xenon lamp solar simulator (Oriel) delivering 100 mW/cm² (AM 1.5G), with light intensity continuously monitored by a silicon photodiode. The cell temperature was maintained at 25 °C, and the voltage sweep rate was 20 mV/s. A metal mask defined the active area of the device, which was 0.06 cm². Surface morphology of the control and passivated perovskite samples was analyzed using scanning electron microscopy (SEM, JCM-6000Plus).

CHAPTER FOUR

4. RESULTS AND DISCUSSION

4.1. XRD data analysis

The perovskite active layer samples in structure of ITO/$Cs_{0.05}(MA_{0.02}FA_{0.98})_{0.95}Pb(I_{0.98}Br_{0.02})_3$ and ITO/$Cs_{0.05}(MA_{0.02}FA_{0.98})_{0.95}Pb(I_{0.98}Br_{0.02})_3$ /PEAI were fabricated at the same spinning rate of 4000 rpm to study the structural effect of PEAI salt on 3D perovskite by XRD. The XRD graph of control and PEAI passivated samples are showed in Figure 18 a. The control sample shows characteristic diffraction peaks at 2θ values of approximately 14°, 20°, 24°, 28°, and 31°. The presence of these major peaks and the absence of any impurity indicate the successful formation of pure perovskite phase without secondary phases in the bulk. After PEAI surface passivation, a new diffraction peak formed at a low 2θ angle of approximately 5.3°. This peak is indicative of the formation of a 2D layered perovskite phase, PEA_2PbI_4, at the surface of the 3D perovskite film (Jiang et al., 2019). According to previous reports, including Li et al., (2021) and others, such low angle peak (below 10°) are behaviour of Ruddlesden–Popper type 2D perovskites formed via the reaction of excess PbI_2 with bulky organic cations like PEA^+ (Li et al., 2021). The appearance of the peak at 5.3° strongly suggests the successful formation of PEA_2PbI_4 on the surface of the 3D perovskite film due PEAI reaction with excess PbI_2 (Zhai et al., 2021). The main characteristic peak formed around 2θ of 13.4° is shift slightly to a lower angle in the PEAI passivated sample compared to the control as in figure 18 b. This shift suggest a change in the lattice parameters, possibly due to the intercalation of the larger PEA^+ organic cations into the 3D perovskite lattice, supporting the formation of a 2D/3D hybrid perovskite film (Li et al., 2023). To analysis the effect of PEAI passivation on the crystallite size, the Scherrer equation (equation 3) was applied to the major diffraction peak as shown in table 2 and 3 for passivated and control sample respectively. From scherrer equation calculation an average crystallite size of 37.04 and 50.16 nm were obtained for the control and passivated samples respectively. The improvement in crystallite size suggests that the PEAI passivation not only induces the formation of a 2D perovskite phase but also influences the growth and/or recrystallization of the underlying 3D perovskite grains, leading to larger crystallite domains (Liu et al., 2025).

$$D = K\lambda / (\beta\cos\theta) \ldots\ldots\ldots\ldots\ldots\ldots\ldots\ldots (3)$$

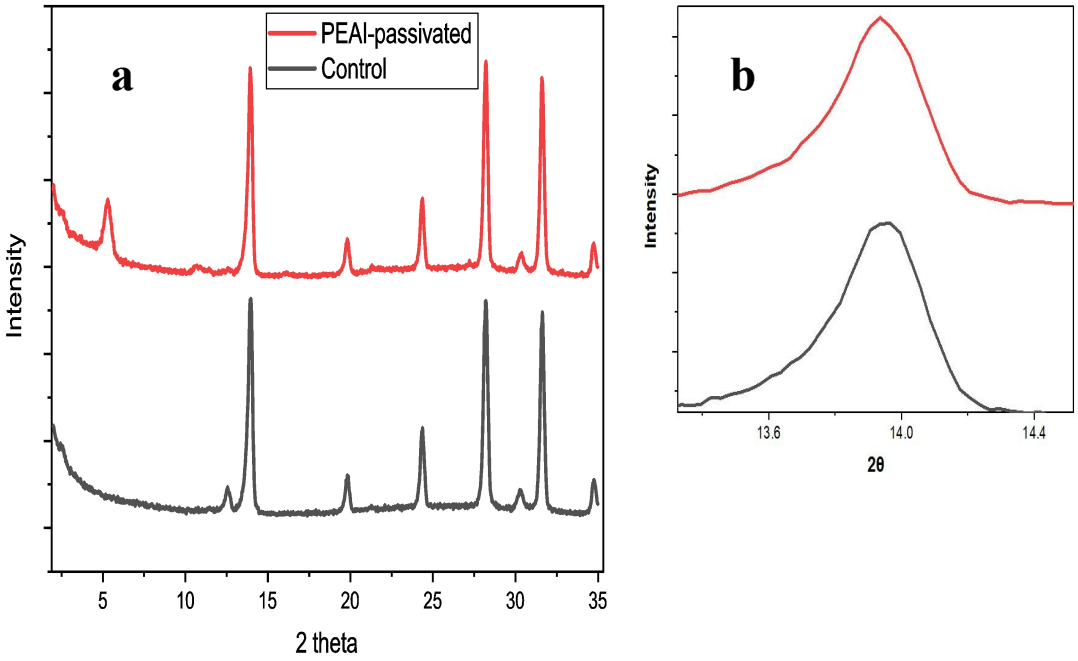

Figure 18. a) XRD pattern of control and PEAI passivated perovskite film, b) the peak position shift of perovskite films.

Table 2. *Crystalline size for passivated film*

Peak Position	FWHM	Crystallite size D nm	average crystallite size
5.29515	0.42788	1.500295367	
13.92353	0.34458	0.570565727	
13.94353	27.37644	0.570565727	
24.34324	0.29707	0.326344768	**0.50**
28.19581	11.15511	0.28175424	
31.61552	0.29186	0.251278138	
34.38656	6.64895	0.231028897	

Table 3. *Crystalline size for control film*

Peak Position	FWHM	Crystallite size D nm	average crystallite size
12.52907	17.72231	0.634068531	
13.97287	0.34355	0.568550986	
19.81589	26.5141	0.400904981	**0.37**
24.36047	0.00577	0.326113947	
28.1686	0.30336	0.282026406	
30.31008	24.60246	0.262100562	
30.40844	1.34E+18	0.261252764	

4.2 UV-Vis spectroscopy measurement

To study the optical properties of both control and passivated samples UV-Vis spectroscopy in the wavelength range of 350 to 950 nm were investigated, as shown in Figure 19 a and b. Both samples show strong absorption in the visible region (400–750 nm), which is in agreement with the high absorption coefficients characteristic of lead halide perovskite materials (Mannar et al., 2022). The average transmittance of 2.9 and 2.7% was found for control and passivated sample in between 500-750nm, which means both samples are highly absorbent in visible region with an absorption threshold wavelength of 750 nm. The incorporation of PEAI does not alter the optical band gap, consistent with previously reported results on similar perovskite systems (Jiang et al., 2021). This suggests that the passivation process preserves the intrinsic optical transitions of the perovskite material. Furthermore, the overall absorption intensity and spectral profile of the two samples are almost similar throughout the measured range. The optical band gap (Eg) of the fabricated samples was determined using the Tauc relation as shown in equation 4 below,

$$(\alpha h\nu)=A(h\nu-Eg)^{n} \quad \ldots\ldots(4)$$

Tauc equation is used to study the optical absorption spectra of semiconducting materials where hν is the photon energy, **α** is the absorption coefficient, and Eg is the band gap, A is a constant and the value of n takes on different values based on the type of optical transition: n=1/2 for allowed direct transitions, n=2 for allowed indirect transitions, n=3/2 for forbidden direct transitions, and n=3 for forbidden indirect transitions. In this study, the value of n=1/2 was used, indicating an allowed direct band gap transition. The optical band gap was then estimated by plotting $(\alpha h\nu)^2$ against hν and extrapolating the linear portion of the plot to the energy axis at the point where $(\alpha h\nu)^2=0$. This approach provides a reliable estimation of the band gap energy, which is a key parameter for understanding the optoelectronic properties of the material.

From Tauc plots, constructed with the assumption of a direct allowed transition(n=2), an optical band gap is approximately 1.58 eV for both the control and passivated samples as indicated in figure 19 c. The agreement in the band gap values indicate PEAI passivation does not significantly alter the electronic structure of the material. The primary role of PEAI lies in reducing defect density and nonradiative

recombination properties rather than modifying the bulk optical behavior of the material (Shi et al., 2024).

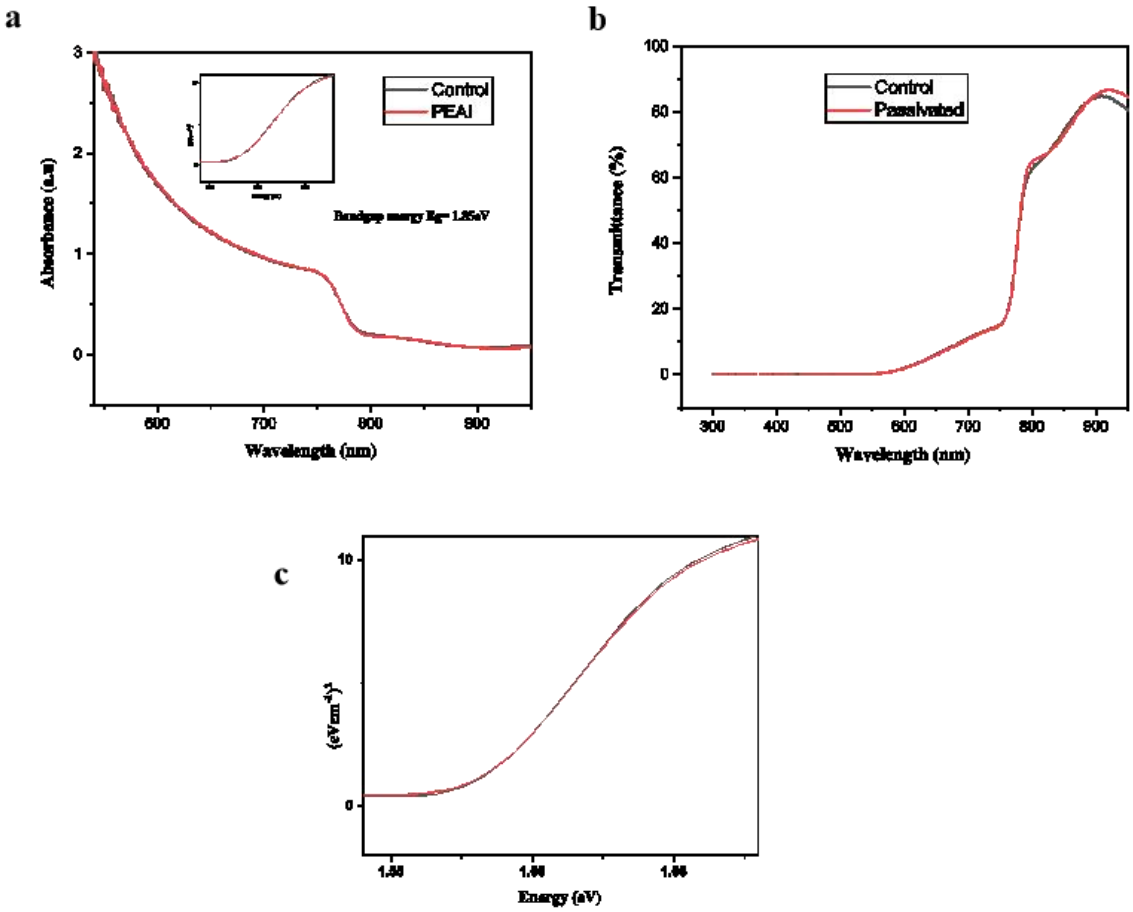

Figure 19. a) UV-vis absorbance spectra of perovskite films grown on ITO. b) Transmittance spectra of perovskite films grown on ITO. c) Tauc plots

4.3 Photoluminescence measurement

The effect of PEAI passivation on the radiative efficiency of both control and passivated samples were investigated by using PL spectroscopy, as indicated in Figure 20. PL measurements were carried out using an excitation wavelength of 520 nm. The PL spectrum shows an enhancement in the PL emission intensity as PEAI passivation applied. This enhancement is associated with suppression of nonradiative recombination pathways within the perovskite material (Cheng et al., 2022). The surface defects of 3D perovskite which is trap states for photogenerated exciton (Xue et al., 2024), are effectively passivated by PEAI passivation. PEAI passivation

reduces the probability of charge carriers recombining nonradiatively, so that leading to a higher radiative recombination and thus a more intense PL emission. This finding corroborates with the improved device performance observed in the J-V characteristics Table 2, higher Voc and FF in the PEAI-treated devices can be attributed to the reduced charge carrier losses resulting from effective PEAI-induced surface defect passivation.

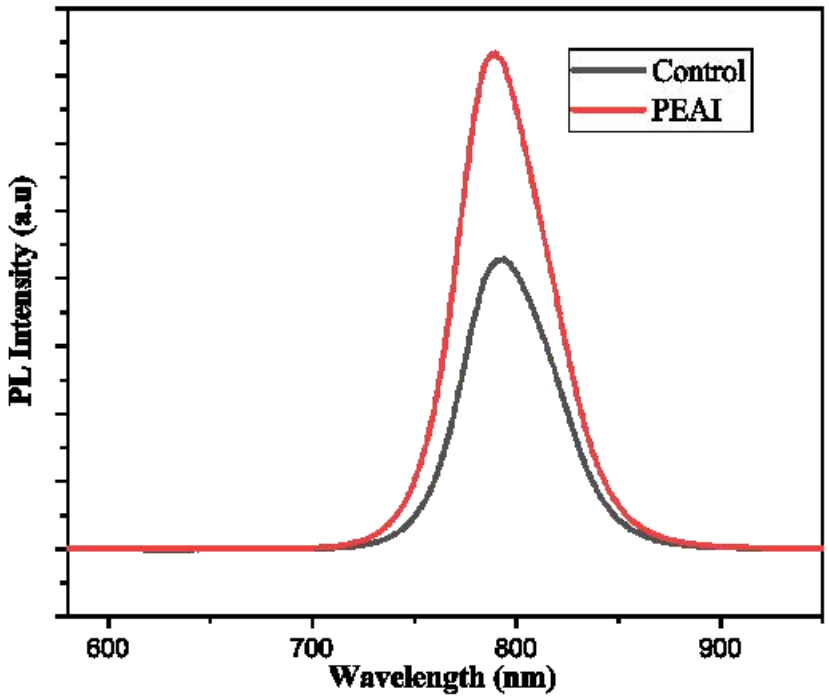

Figure 20. Photoluminiscence of control and PEAI passivated perovskite film.

4.4 Electroluminescence measurement

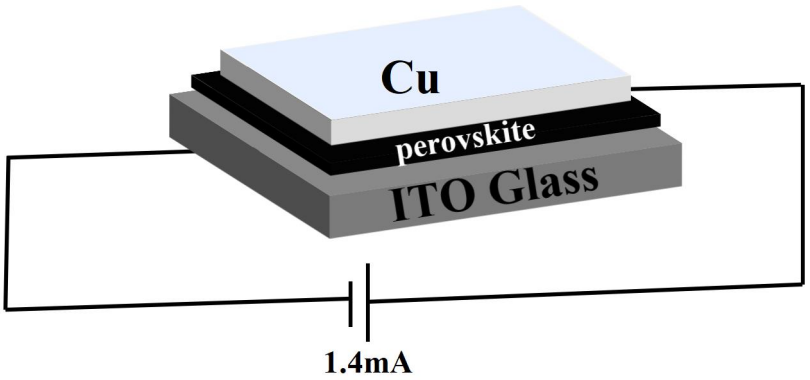

Figure 21. The schematic of an EL sample *preparation* by *sandwiching* $Cs_{0.05}(MA_{0.02}FA_{0.98})_{0.95}Pb(I_{0.98}Br_{0.02})_3$ in between ITO-coated glass plates and Cu electrode.

The electroluminescence (EL) characterization was performed for both control and PEAI passivated samples as illustrated in figure 21, with applied current of 1.4mA which is equivalent to short circuit current, Isc, to the samples. The EL emission shown in Figure 22 a. give important information on the radiative recombination behavior of PSCs under working conditions. The active layer of these devices consists of the $Cs_{0.05}(FA_{0.98}MA_{0.02})_{0.95}Pb(I_{0.98}Br_{0.02})_3$. The EL emission peak appeared at around 780 nm irrespective of the device type, which is characteristic emission of the perovskite layer under an applied bias. This is in agreement with the maximum peak where the PL emission peak occurred. The PEAI treated device show a increase in EL intensity across the spectrum, with a significantly higher peak intensity compared the control sample. Zhuang, J., et al., found that there are many surface defects available on the surface of 3D perovskite, including undercoordinated Pb^{2+}/I^- ions, MA/I vacancy, and occasionally Pb−I antisite substitution (Zhuang et al., 2019). The enhancement in EL intensity likely indicates the suppression of nonradiative recombination due to surface defect within the working device as a result of PEAI surface passivation (Cheng et al., 2022). The PEAI form chemical reaction with uncoordinated lead (Pb^{2+}) or formamide (FA^+) ions on the 3D perovskite surface, as a result it deactivate those defects and reduce nonradiative recombination. This improvement in EL correlates well with the observed increase in device performance parameters such as Voc and FF, highlighting the importance of surface passivation for achieving high-efficiency perovskite solar cells.

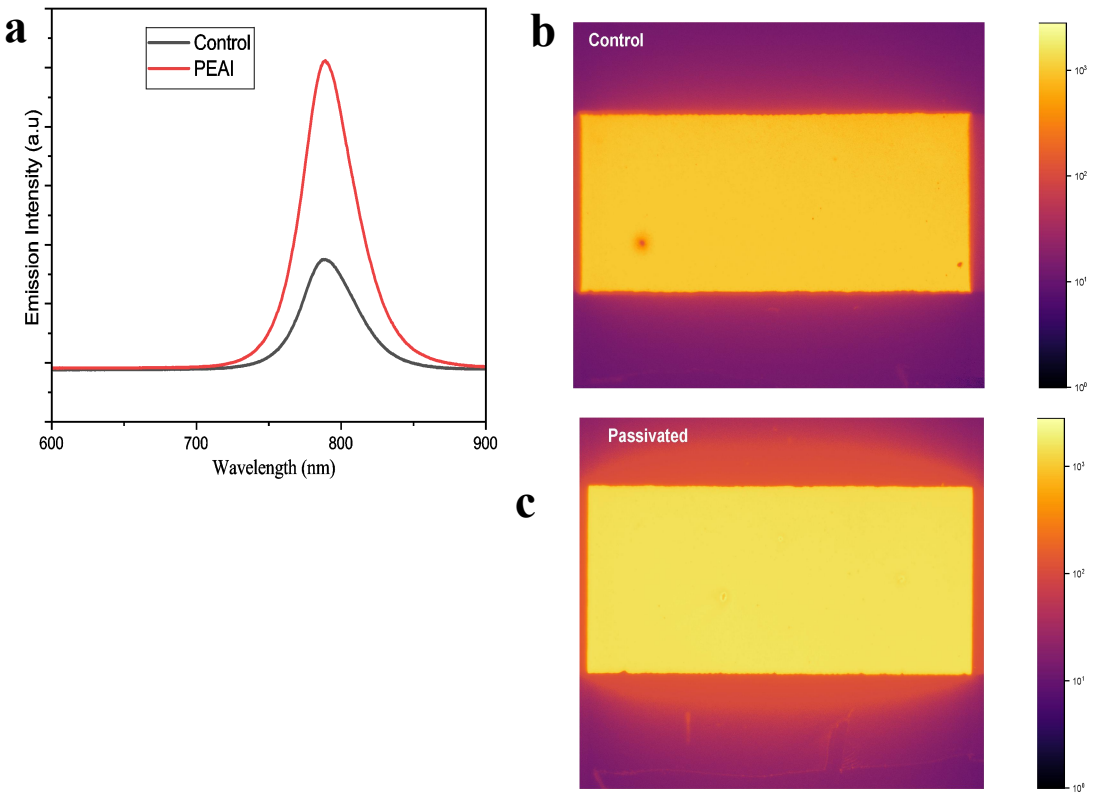

Figure 22. a) Electroluminescence spectrum of passivated and non-passivated perovskite film b) Electroluminescence imaging for control, and c) Passivated devices

As shown in Figure 22b and 22c, electroluminescence (EL) imaging reveals a noticeable increase in EL emission after PEAI passivation. This enhancement is primarily attributed to suppressed nonradiative recombination, allowing radiative recombination to dominate. The control device exhibits weak EL emission, indicating significant carrier losses due to nonradiative pathways. In contrast, the PEAI-passivated device displays brighter and more uniform EL across the active area, suggesting effective defect passivation. This spatial uniformity and increased brightness imply reduced trap-assisted recombination and improved light emission efficiency. The enhanced EL observed in the imaging is consistent with the higher EL intensity in the emission spectrum, further confirming the role of PEAI in improving the optoelectronic quality of the perovskite layer and contributing to better overall device performance.

4.5 Scanning electron microscopy image of perovskite film

To analysis the effect PEAI passivation on the surface morphology of perovskite active layer, both control and passivated films are characterized with SEM, as shown in Figure 23. As clearly indicated in figure 23 a, the control perovskite film shows rough surface, visible grain boundaries, and the presence of voids and pinholes, those surface properties are often associated with nonradiative recombination sites and inefficient charge transport (Yang et al., 2017). In contrast, the passivated film exhibits uniform grain, smoother surface, and fewer voids, which is possibly due to suppressed for pinhole induced nonradaitive recombination in agreement with Voc and FF of their device, as indicated in figure 23 b. Those surface morphology improvement indicates the PEAI treatment was effectively passivates surface and grain boundary defects, likely through the electrostatic interaction of the phenylethylammonium cation with undercoordinated lead or halide ions (Zhuang et al., 2019). Moreover, the control film is more brighter than passivated film, which is most likely due to the less conductivity of 2D perovskite layer on top of 3D. The improved surface properties of the PEAI-treated film agree well with enhanced optoelectronic properties observed in photoluminescence and device performance measurements.

a) **b)**

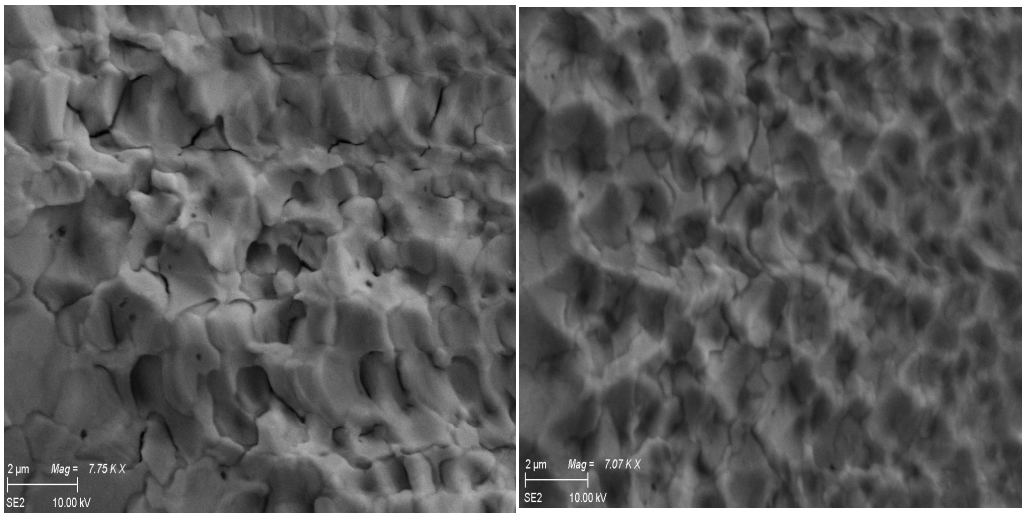

Figure 23: SEM images of perovskite films: (a) Control, (b) PEAI-treated.

4.6 Photovoltaic performance of devices

Effect of PEAI treatment on current density (J)-voltage (V) curves of PSCs device is shown in Figure 24, and all photovoltaic parameters are listed in Table 4.

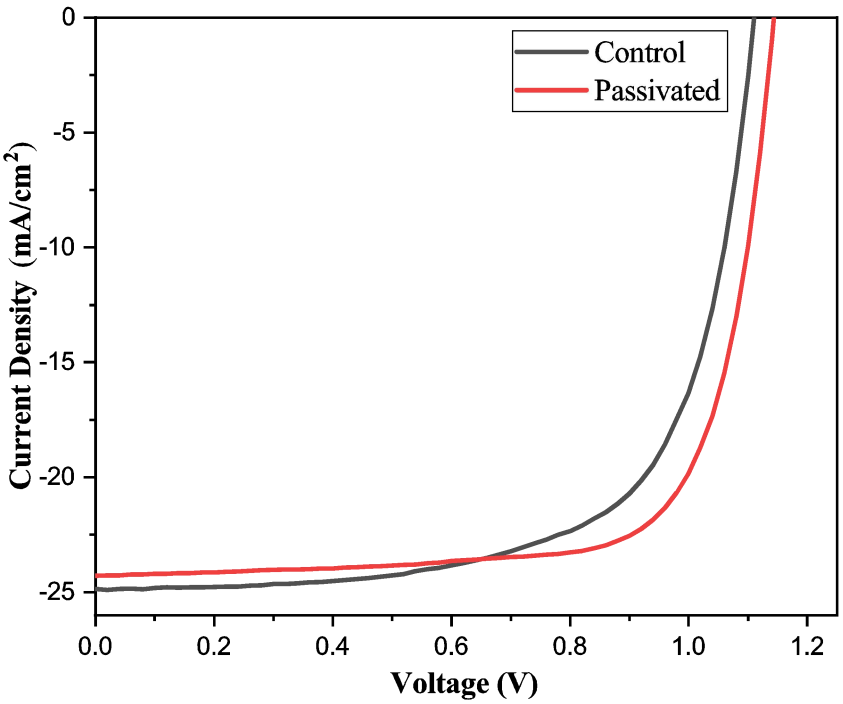

Figure 24. J-V curves of control and PEAI treated PSCs devices.

The J–V curve of both control and PEAI-passivated PSCs, as shown in Figure 24, shows the enhancement in device performance following PEAI surface passivation. Upon PEAI passivation, key photovoltaic parameters, specifically the open-circuit voltage (Voc) and fill factor (FF), show significant improvement. Voc increases from 1.10 V to 1.15 V, and FF improves from 67.6% to 71.9% when comparing the control device to the PEAI-passivated device. These enhancements are attributed to the effective suppression of charge carrier recombination and a corresponding reduction in voltage losses (Chen et al., 2022). The improvement of those photovoltaic parameters highlights the significant role of passivation, as device performance is influenced by surface defect mitigation. In particular, the enhancements in Voc and FF are believed to stem from the reduction of surface defects, which effectively suppress charge recombination (Zhuang et al., 2019).

These improvements are also supported by PL and EL measurements, where the passivated films show enhanced emission intensities, as a result of effective mitigation of nonradiative recombination pathways(Cheng et al., 2022).

From the XRD analysis also the structural enhancement induced by PEAI passivation is observed. Upon the PEAI treatment the crystallite size of the film was enhanced, so as the crystallite size become higher and higher the grain boundary density become reduced and which are directly associated with nonradiative recombination center. Consequently, The overall PCE increased by approximately 9% upon PEAI passivation from 18.9% to 20.6%. While the Jsc experienced a slight decrease from 24.8 mA/cm² to 24.4 mA/cm², the improvements in Voc and FF more than compensated for this, resulting in superior device performance.

Table 4. S*ummary of performance of control and PEAI passivated PSCs device.*

PV Parameters	Control device	Passivated device
J_{sc} (mA/cm^2)	24.8	24.4
V_{oc} (V)	1.1	1.15
FF (%0	67.6	71.9
PCE (%)	18.9	20.6

4.7 External quantum efficiency analysis

To further analysis the device photovoltaic properties of both device the external quantum efficiency was performed for wavelengths between 300 nm to 1000 nm in 5 nm increments, as shown in Figure 25. The PEAI-passivated device and the control device shows comparable EQE response throughout most of the visible wavelength range (Jiang et al., 2019).

The current density derived from the EQE spectrum for the PEAI-treated device is slightly lower than that of the control, consistent with the minor decrease in Jsc from 24.8 mA/cm² to 24.4 mA/cm² observed in the J–V characteristics. This small drop in short-circuit current density may be attributed to the formation of a thin 2D PEA_2PbI_4, which, while beneficial for defect passivation, but slightly hinder charge extraction or introduce optical losses . Nevertheless, the gain in open-circuit voltage (Voc) and fill

factor (FF) outweighs this loss, resulting in a net enhancement of the power conversion efficiency (PCE) from 18.9% to 20.6%.

From these findings the PEAI treatment does not significantly affect the optical properties rather than enhances device performance by mitigating nonradiative recombination pathways and improving interfacial quality. This aligns with previous reports where quasi-2D/3D hybrid perovskite structures achieved higher Voc and FF due to superior passivation and reduced surface recombination (Zhang & Park, 2022).

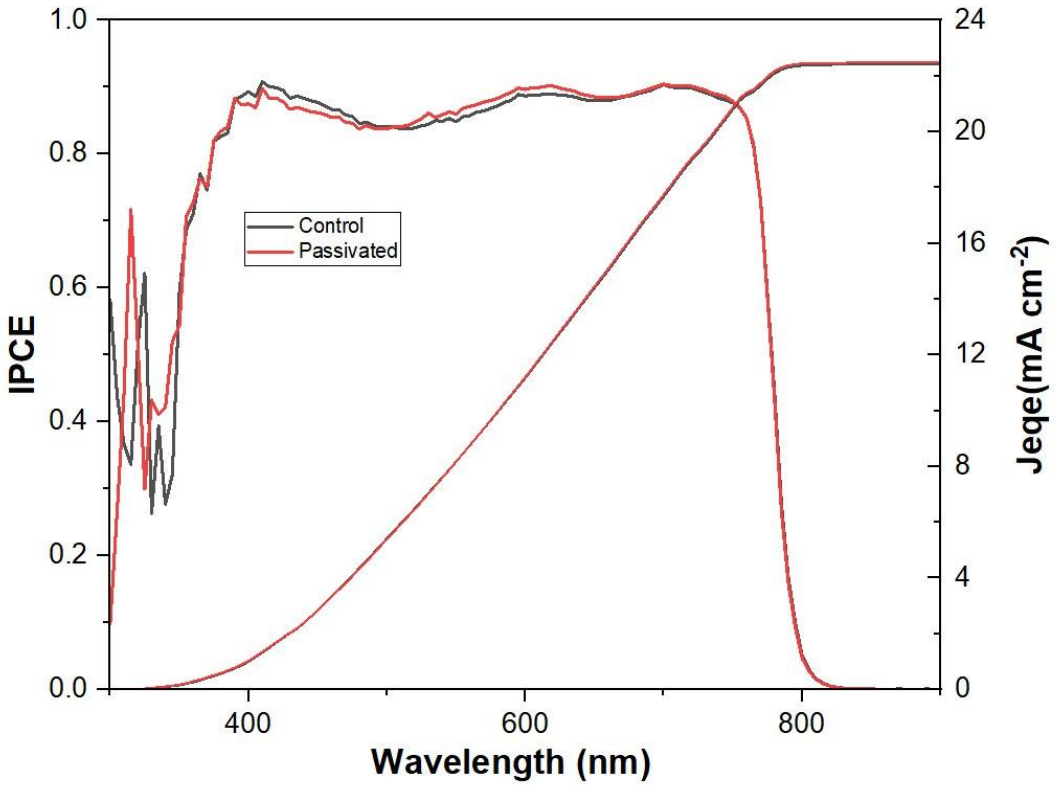

Figure 25. The external quantum efficiency (EQE) spectra of both the control and PEAI passivated PSCs.

Conclusion

This thesis strategically investigated the use of phenethylammonium iodide (PEAI) for surface passivation to enhance the performance of perovskite solar cells (PSCs). The perovskite absorber layer with the composition $Cs_{0.05}(MA_{0.02}FA_{0.98})_{0.95}Pb(I_{0.98}Br_{0.02})_3$ was successfully synthesized and characterized by XRD, UV-Vis, PL, EL, and SEM techniques. The introduction of a PEAI passivation layer applied without post-annealing led to a noticeable reduction in surface defect density and suppression of nonradiative recombination. This was evidenced by enhanced photoluminescence emission and reduced trap-assisted recombination, ultimately contributing to improved device performance. Device fabrication using an inverted planar architecture ITO/MeO-2PACz/perovskite/PEAI/C_{60}/BCP/Cu showed the effectiveness of this surface engineering approach. In comparison to the control device, which showed a PCE of 18.9%, the device treated with PEAI achieved a higher PCE of 20.6%. This performance enhancement indicate how important surface passivation is in minimizing energy losses and improving the movement of charge carriers within the device. The XRD data analysis revealed the formation of a low-angle XRD peak (~5.3°), indicating the formation of a thin 2D perovskite layer (PEA_2PbI_4) on the surface, which contributed to defect passivation without significantly affecting charge transport. Overall, this work confirms that direct surface passivation with PEAI, without additional post annealing treatment, is a straightforward yet highly effective strategy to enhance the efficiency of triple cation PSCs.

Reference

Abiram, G., Thanihaichelvan, M., Ravirajan, P., & Velauthapillai, D. (2022). Review on perovskite semiconductor field–effect transistors and their applications. *Nanomaterials*, *12*(14), 2396.

Adhikari, R. D., Patel, M. J., Baishya, H., Yadav, D., Kalita, M., Alam, M., & Iyer, P. K. (2025). Decoding recombination dynamics in perovskite solar cells: an in-depth critical review. *Chemical Society Reviews*.

Ahmad, W., Khan, J., Niu, G., & Tang, J. (2017). Inorganic CsPbI3 perovskite-based solar cells: A choice for a tandem device. *Solar RRL*, *1*(7), 1700048.

Ahmed, A., Riaz, K., Mehmood, H., Tauqeer, T., & Ahmad, Z. (2020). Performance optimization of CH3NH3Pb (I1-xBrx) 3 based perovskite solar cells by comparing different ETL materials through conduction band offset engineering. *Optical Materials*, *105*, 109897.

Akin, S., Dong, B., Pfeifer, L., Liu, Y., Graetzel, M., & Hagfeldt, A. (2021). Organic ammonium halide modulators as effective strategy for enhanced perovskite photovoltaic performance. *Advanced Science*, *8*(10), 2004593.

Al-Mousoi, A. K., Mohammed, M. K., Kumar, A., Pandey, R., Madan, J., Dastan, D., Hossain, M. K., Sakthivel, P., & Yaseen, Z. M. (2023). Understanding Auger recombination in perovskite solar cells. *Physical Chemistry Chemical Physics*, *25*(24), 16459-16468.

Albaladejo-Siguan, M., Becker-Koch, D., Taylor, A. D., Sun, Q., Lami, V., Oppenheimer, P. G., Paulus, F., & Vaynzof, Y. (2019). Efficient and stable PbS quantum dot solar cells by triple-cation perovskite passivation. *ACS nano*, *14*(1), 384-393.

Almalki, F. A., Alsamhi, S. H., Sahal, R., Hassan, J., Hawbani, A., Rajput, N., Saif, A., Morgan, J., & Breslin, J. (2023). Green IoT for eco-friendly and sustainable smart cities: future directions and opportunities. *Mobile Networks and Applications*, *28*(1), 178-202.

Amjith, L., & Bavanish, B. (2022). A review on biomass and wind as renewable energy for sustainable environment. *Chemosphere*, *293*, 133579.

An, Y., Hidalgo, J., Perini, C. A. R., Castro-Mendez, A.-F., Vagott, J. N., Bairley, K., Wang, S., Li, X., & Correa-Baena, J.-P. (2021). Structural stability of

formamidinium-and cesium-based halide perovskites. *ACS Energy Letters*, *6*(5), 1942-1969.

Andrew, R. M. (2020). A comparison of estimates of global carbon dioxide emissions from fossil carbon sources. *Earth System Science Data*, *12*(2), 1437-1465.

Ang, T.-Z., Salem, M., Kamarol, M., Das, H. S., Nazari, M. A., & Prabaharan, N. (2022). A comprehensive study of renewable energy sources: Classifications, challenges and suggestions. *Energy strategy reviews*, *43*, 100939.

Ansari, M. I. H., Qurashi, A., & Nazeeruddin, M. K. (2018). Frontiers, opportunities, and challenges in perovskite solar cells: A critical review. *Journal of Photochemistry and Photobiology C: Photochemistry Reviews*, *35*, 1-24. https://doi.org/https://doi.org/10.1016/j.jphotochemrev.2017.11.002

Asghar, M. I., Zhang, J., Wang, H., & Lund, P. D. (2017). Device stability of perovskite solar cells–A review. *Renewable and Sustainable Energy Reviews*, *77*, 131-146.

Askar, A. M., Bernard, G. M., Wiltshire, B., Shankar, K., & Michaelis, V. K. (2017). Multinuclear magnetic resonance tracking of hydro, thermal, and hydrothermal decomposition of CH3NH3PbI3. *The Journal of Physical Chemistry C*, *121*(2), 1013-1024.

Ašmontas, S., Čerškus, A., Gradauskas, J., Grigucevičienė, A., Leinartas, K., Lučun, A., Petrauskas, K., Selskis, A., Sužiedėlis, A., & Širmulis, E. (2021). Cesium-containing triple cation perovskite solar cells. *Coatings*, *11*(3), 279.

Ava, T. T., Al Mamun, A., Marsillac, S., & Namkoong, G. (2019). A review: thermal stability of methylammonium lead halide based perovskite solar cells. *Applied Sciences*, *9*(1), 188.

Bi, E., Chen, H., Xie, F., Wu, Y., Chen, W., Su, Y., Islam, A., Grätzel, M., Yang, X., & Han, L. (2017). Diffusion engineering of ions and charge carriers for stable efficient perovskite solar cells. *Nature communications*, *8*(1), 15330.

Bonadio, A., Sabino, F. P., Freitas, A. L., Felez, M. R., Dalpian, G. M., & Souza, J. A. (2023). Comparing the cubic and tetragonal phases of mapbi3 at room temperature. *Inorganic Chemistry*, *62*(19), 7533-7544.

Braid, J. L. (2016). *Understanding efficiency improvement in organic photovoltaics with molecular modifiers*. Colorado School of Mines.

Bulowski, W., Szwanda, A., Gawlińska-Nęcek, K., Panek, P., Lipiński, M., Janusz-Skuza, M., Szczerba, M. J., Majchrowicz, Ł., Mahapatra, A., & Prochowicz, D.

(2024). Optimization of the ETL titanium dioxide layer for inorganic perovskite solar cells. *Journal of Materials Science*, *59*(17), 7283-7298.

Calado, P., Telford, A. M., Bryant, D., Li, X., Nelson, J., O'Regan, B. C., & Barnes, P. R. (2016). Evidence for ion migration in hybrid perovskite solar cells with minimal hysteresis. *Nature communications*, *7*(1), 13831.

Cao, Z., Li, C., Deng, X., Wang, S., Yuan, Y., Chen, Y., Wang, Z., Liu, Y., Ding, L., & Hao, F. (2020). Metal oxide alternatives for efficient electron transport in perovskite solar cells: Beyond TiO 2 and SnO 2. *Journal of Materials Chemistry A*, *8*(38), 19768-19787.

Chen, B., Wang, S., Zhang, X., Zhu, W., Cao, Z., & Hao, F. (2022). Reducing the interfacial voltage loss in tin halides perovskite solar cells. *Chemical Engineering Journal*, *445*, 136769.

Chen, B., Yang, M., Priya, S., & Zhu, K. (2016). Origin of J–V hysteresis in perovskite solar cells. *The journal of physical chemistry letters*, *7*(5), 905-917.

Chen, H., Chen, Y., Zhang, T., Liu, X., Wang, X., & Zhao, Y. (2021). Advances to high-performance black-phase FAPbI3 perovskite for efficient and stable photovoltaics. *Small Structures*, *2*(5), 2000130.

Chen, S.-C., Wang, D., & Zheng, Q. (2020). Surface passivation of all-inorganic CsPbI2Br with a fluorinated organic ammonium salt for perovskite solar cells with efficiencies over 16%. *Solar RRL*, *4*(10), 2000321.

Chen, Y., Meng, Q., Zhang, L., Han, C., Gao, H., Zhang, Y., & Yan, H. (2019). SnO2-based electron transporting layer materials for perovskite solar cells: A review of recent progress. *Journal of energy chemistry*, *35*, 144-167.

Cheng, H., Feng, Y., Fu, Y., Zheng, Y., Shao, Y., & Bai, Y. (2022). Understanding and minimizing non-radiative recombination losses in perovskite light-emitting diodes. *Journal of Materials Chemistry C*, *10*(37), 13590-13610.

Cho, K. T., Zhang, Y., Orlandi, S., Cavazzini, M., Zimmermann, I., Lesch, A., Tabet, N., Pozzi, G., Grancini, G., & Nazeeruddin, M. K. (2018). Water-repellent low-dimensional fluorous perovskite as interfacial coating for 20% efficient solar cells. *Nano letters*, *18*(9), 5467-5474.

Christians, J. A., Miranda Herrera, P. A., & Kamat, P. V. (2015). Transformation of the excited state and photovoltaic efficiency of CH3NH3PbI3 perovskite upon controlled exposure to humidified air. *Journal of the American Chemical Society*, *137*(4), 1530-1538.

Chung, I., Song, J.-H., Im, J., Androulakis, J., Malliakas, C. D., Li, H., Freeman, A. J., Kenney, J. T., & Kanatzidis, M. G. (2012). CsSnI3: semiconductor or metal? High electrical conductivity and strong near-infrared photoluminescence from a single material. High hole mobility and phase-transitions. *Journal of the American Chemical Society*, *134*(20), 8579-8587.

Degani, M., An, Q., Albaladejo-Siguan, M., Hofstetter, Y. J., Cho, C., Paulus, F., Grancini, G., & Vaynzof, Y. (2021). 23.7% Efficient inverted perovskite solar cells by dual interfacial modification. *Science advances*, *7*(49), eabj7930.

Deshmukh, M. K. G., Sameeroddin, M., Abdul, D., & Sattar, M. A. (2023). Renewable energy in the 21st century: A review. *Materials today: proceedings*, *80*, 1756-1759.

Devasia, S. (2023). *Ultrasonic spray deposition of perovskite-inspired lead-free cesium bismuth iodide thin films for optoelectronics* Universidad Autónoma de Nuevo León].

Dey, K., Roose, B., & Stranks, S. D. (2021). Optoelectronic properties of low-bandgap halide perovskites for solar cell applications. *Advanced Materials*, *33*(40), 2102300.

Dipta, S. S., Howlader, A. H., Tarique, W. B., & Uddin, A. (2024). Comparative analysis of the stability and performance of double-, triple-, and quadruple-cation perovskite solar cells for rooftop and indoor applications. *Molecules*, *29*(12), 2758.

Duan, L., & Uddin, A. (2022). Defects and stability of perovskite solar cells: a critical analysis. *Materials Chemistry Frontiers*, *6*(4), 400-417.

El-Afifi, M. I. (2024). Solar Energy: Our Future for Sustainable Energy. *Nile Journal of Communication and Computer Science*, *7*(1), 67-83.

Fan, Y., Meng, H., Wang, L., & Pang, S. (2019). Review of stability enhancement for formamidinium-based perovskites. *Solar RRL*, *3*(9), 1900215.

Frost, J. M., Butler, K. T., Brivio, F., Hendon, C. H., Van Schilfgaarde, M., & Walsh, A. (2014). Atomistic origins of high-performance in hybrid halide perovskite solar cells. *Nano letters*, *14*(5), 2584-2590.

Fu, L., Li, H., Wang, L., Yin, R., Li, B., & Yin, L. (2020). Defect passivation strategies in perovskites for an enhanced photovoltaic performance. *Energy & Environmental Science*, *13*(11), 4017-4056.

Fu, Y., Zhu, H., Chen, J., Hautzinger, M. P., Zhu, X.-Y., & Jin, S. (2019). Metal halide perovskite nanostructures for optoelectronic applications and the study of physical properties. *Nature Reviews Materials*, *4*(3), 169-188.

Fung, D. D., & Choy, W. C. (2013). Experimental studies of plasmonic nanoparticle effects on organic solar cells. In *Organic Solar Cells* (pp. 211-242). Springer.

Gehrig, D. (2015). *Unraveling efficiency-limiting processes in organic solar cells by ultrafast spectroscopy-impact of chemical structure and morphology on photophysics and efficency* Johannes Gutenberg-Universität Mainz].

Gong, Z., Wang, R., Jiang, Y., Kong, X., Lin, Y., Xu, Z., Zhou, G., Liu, J.-M., Kempa, K., & Gao, J. (2021). Novel DAD type small-molecular hole transport materials for stable inverted perovskite solar cells. *Organic Electronics*, *92*, 106102.

Grancini, G., Roldán-Carmona, C., Zimmermann, I., Mosconi, E., Lee, X., Martineau, D., Narbey, S., Oswald, F., De Angelis, F., & Graetzel, M. (2017). One-Year stable perovskite solar cells by 2D/3D interface engineering. *Nature communications*, *8*(1), 15684.

Grandhi, G. K., Hardy, D., Krishnaiah, M., Vargas, B., Al-Anesi, B., Suryawanshi, M. P., Solis-Ibarra, D., Gao, F., Hoye, R. L., & Vivo, P. (2024). Wide-bandgap perovskite-inspired materials: defect-driven challenges for high-performance optoelectronics. *Advanced Functional Materials*, *34*(50), 2307441.

Green, M. A., Ho-Baillie, A., & Snaith, H. J. (2014). The emergence of perovskite solar cells. *Nature photonics*, *8*(7), 506-514.

Gu, X., Xiang, W., Tian, Q., & Liu, S. (2021). Rational surface-defect control via designed passivation for high-efficiency inorganic perovskite solar cells. *Angewandte Chemie International Edition*, *60*(43), 23164-23170.

Gutierrez-Partida, E., Hempel, H., Caicedo-Dávila, S., Raoufi, M., Peña-Camargo, F., Grischek, M., Gunder, R., Diekmann, J., Caprioglio, P., & Brinkmann, K. O. (2021). Large-grain double cation perovskites with 18 μs lifetime and high luminescence yield for efficient inverted perovskite solar cells. *ACS Energy Letters*, *6*(3), 1045-1054.

Guvenc, C. M., Toso, S., Ivanov, Y. P., Saleh, G., Balci, S., Divitini, G., & Manna, L. (2024). Breaking the Boundaries of the Goldschmidt Tolerance Factor with Ethylammonium Lead Iodide Perovskite Nanocrystals. *ACS nano*, *19*(1), 1557-1565.

Hafezi, R., & Alipour, M. (2021). Renewable energy sources: traditional and modern-age technologies. In *Affordable and clean energy* (pp. 1085-1099). Springer.

He, J., Chu, Y., Sun, Y., Zhang, R., Li, J., Zhao, L., Zhao, H., Liu, P., & Li, S. (2021). Beyond the Limit of Goldschmidt Tolerance Factor: Crystal Surface Engineering to Boost the α-Phase Stability of Formamidinium-Only Hybrid Inorganic–Organic Perovskites. *Solar RRL*, *5*(8), 2100188.

He, R., Ren, S., Chen, C., Yi, Z., Luo, Y., Lai, H., Wang, W., Zeng, G., Hao, X., & Wang, Y. (2021). Wide-bandgap organic–inorganic hybrid and all-inorganic perovskite solar cells and their application in all-perovskite tandem solar cells. *Energy & Environmental Science*, *14*(11), 5723-5759.

Hettiarachchi, C., Srikanth, H., Karaiskaj, D., & Phan, M.-H. (2015). Perovskite Solar Absorbers and Ferroelectric Nanocomposites For Harvesting Solar Energy.

Hoppe, H., & Sariciftci, N. S. (2004). Organic solar cells: An overview. *Journal of materials research*, *19*(7), 1924-1945.

Hossain, M. K., Toki, G. I., Kuddus, A., Rubel, M. H., Hossain, M., Bencherif, H., Rahman, M. F., Islam, M. R., & Mushtaq, M. (2023). An extensive study on multiple ETL and HTL layers to design and simulation of high-performance lead-free CsSnCl3-based perovskite solar cells. *Scientific reports*, *13*(1), 2521.

Howard, J. M., Wang, Q., Srivastava, M., Gong, T., Lee, E., Abate, A., & Leite, M. S. (2022). Quantitative predictions of moisture-driven photoemission dynamics in metal halide perovskites via machine learning. *The journal of physical chemistry letters*, *13*(9), 2254-2263.

Hu, Y., Qiu, T., Bai, F., Ruan, W., & Zhang, S. (2018). Highly efficient and stable solar cells with 2D MA3Bi2I9/3D MAPbI3 heterostructured perovskites. *Advanced Energy Materials*, *8*(19), 1703620.

Huang, H., Zhang, X., Zhou, W., Huang, Y., Zheng, Z., Chen, X., Zhang, Y., & Yan, H. (2024). Interface passivation strategies for high-performance perovskite solar cells using two-dimensional perovskites. *Materials Chemistry Frontiers*, *8*(21), 3528-3557.

Iagher, L., & Etgar, L. (2018). Effect of Cs on the stability and photovoltaic performance of 2D/3D perovskite-based solar cells. *ACS Energy Letters*, *3*(2), 366-372.

Ishikawa, R., Ueno, K., & Shirai, H. (2020). Improved efficiency of methylammonium-free perovskite thin film solar cells by fluorinated ammonium iodide treatment. *Organic Electronics*, *78*, 105596.

Jaiswal, K. K., Chowdhury, C. R., Yadav, D., Verma, R., Dutta, S., Jaiswal, K. S., & Karuppasamy, K. S. K. (2022). Renewable and sustainable clean energy development and impact on social, economic, and environmental health. *Energy Nexus*, *7*, 100118.

Jeon, N. J., Na, H., Jung, E. H., Yang, T.-Y., Lee, Y. G., Kim, G., Shin, H.-W., Il Seok, S., Lee, J., & Seo, J. (2018). A fluorene-terminated hole-transporting material for highly efficient and stable perovskite solar cells. *Nature Energy*, *3*(8), 682-689.

Jiang, Q., Zhao, Y., Zhang, X., Yang, X., Chen, Y., Chu, Z., Ye, Q., Li, X., Yin, Z., & You, J. (2019). Surface passivation of perovskite film for efficient solar cells. *Nature photonics*, *13*(7), 460-466.

Jiang, T., Yang, Y., Hao, X., Fan, J., Wu, L., Wang, W., Zeng, G., Halim, M. A., & Zhang, J. (2024). Self-Assembled Monolayer Hole Transport Layers for High-Performance and Stable Inverted Perovskite Solar Cells. *Energy & Fuels*, *38*(21), 21371-21381.

Jiang, X., Chen, S., Li, Y., Zhang, L., Shen, N., Zhang, G., Du, J., Fu, N., & Xu, B. (2021). Direct surface passivation of perovskite film by 4-fluorophenethylammonium iodide toward stable and efficient perovskite solar cells. *ACS applied materials & interfaces*, *13*(2), 2558-2565.

Jung, H. R., Cho, Y., & Jo, W. (2022). UV and visible photodetectors of MAPbBr3 and MAPbCl3 perovskite single crystals via single photocarrier transport design. *Advanced Optical Materials*, *10*(7), 2102175.

Kahandal, S. S., Tupke, R. S., Bobade, D. S., Kim, H., Piao, G., Sankapal, B. R., Said, Z., Pagar, B. P., Pawar, A. C., & Kim, J. M. (2024). Perovskite solar cells: fundamental aspects, stability challenges, and future prospects. *Progress in Solid State Chemistry*, 100463.

Ke, X., Yan, J., Zhang, A., Zhang, B., & Chen, Y. (2015). Optical band gap transition from direct to indirect induced by organic content of CH3NH3PbI3 perovskite films. *Applied Physics Letters*, *107*(9).

Kheralla, A., & Chetty, N. (2021). A review of experimental and computational attempts to remedy stability issues of perovskite solar cells. *Heliyon*, *7*(2).

Kim, J. Y., Lee, J.-W., Jung, H. S., Shin, H., & Park, N.-G. (2020). High-efficiency perovskite solar cells. *Chemical reviews*, *120*(15), 7867-7918.

Kim, K., Moon, T., & Kim, J. (2025). Wide Bandgap Perovskites: A Comprehensive Review of Recent Developments and Innovations. *Small*, 2407007.

Kore, B. P., Jamshidi, M., & Gardner, J. M. (2024). The impact of moisture on the stability and degradation of perovskites in solar cells. *Materials Advances*, *5*(6), 2200-2217.

Kour, P. P. (2023). Rational design and synthesis of low-dimensional halide perovskites with improved ambient air stability for optoelectronic applications.

Kumar, S., & Rathore, K. (2023). Renewable energy for sustainable development goal of clean and affordable energy. *International Journal of Materials Manufacturing and Sustainable Technologies*, *2*(1), 1-15.

La-Placa, M.-G., Gil-Escrig, L., Guo, D., Palazon, F., Savenije, T. J., Sessolo, M., & Bolink, H. J. (2019). Vacuum-deposited 2D/3D perovskite heterojunctions. *ACS Energy Letters*, *4*(12), 2893-2901.

Lei, L., Dong, Q., Gundogdu, K., & So, F. (2021). Metal halide perovskites for laser applications. *Advanced Functional Materials*, *31*(16), 2010144.

Li, C., Tscheuschner, S., Paulus, F., Hopkinson, P. E., Kießling, J., Köhler, A., Vaynzof, Y., & Huettner, S. (2016). Iodine migration and its effect on hysteresis in perovskite solar cells. *Advanced Materials*, *28*(12), 2446-2454.

Li, H. (2025). 2 Basics of Perovskite. *Defect Passivation and Doping Engineering for Highly Efficient Perovskite Solar Cells*, 10.

Li, N., Jia, Y., Guo, Y., & Zhao, N. (2022). Ion migration in perovskite light-emitting diodes: mechanism, characterizations, and material and device engineering. *Advanced Materials*, *34*(19), 2108102.

Li, N., Tao, S., Chen, Y., Niu, X., Onwudinanti, C. K., Hu, C., Qiu, Z., Xu, Z., Zheng, G., & Wang, L. (2019). Cation and anion immobilization through chemical bonding enhancement with fluorides for stable halide perovskite solar cells. *Nature Energy*, *4*(5), 408-415.

Li, X., Hoffman, J. M., & Kanatzidis, M. G. (2021). The 2D halide perovskite rulebook: how the spacer influences everything from the structure to optoelectronic device efficiency. *Chemical reviews*, *121*(4), 2230-2291.

Li, X., Wu, Y., Zhang, S., Cai, B., Gu, Y., Song, J., & Zeng, H. (2016). CsPbX3 quantum dots for lighting and displays: room-temperature synthesis,

photoluminescence superiorities, underlying origins and white light-emitting diodes. *Advanced Functional Materials*, *26*(15), 2435-2445.

Li, X., Zhang, P., Li, S., Wasnik, P., Ren, J., Jiang, Q., Xu, B. B., & Murugadoss, V. (2023). Mixed perovskites (2D/3D)-based solar cells: a review on crystallization and surface modification for enhanced efficiency and stability. *Advanced Composites and Hybrid Materials*, *6*(3), 111.

Li, Y., Wang, Y., Xu, Z., Peng, B., & Li, X. (2024). Key Roles of Interfaces in Inverted Metal-Halide Perovskite Solar Cells. *ACS nano*, *18*(16), 10688-10725.

Lin, L., Jiang, L., Li, P., Xiong, H., Kang, Z., Fan, B., & Qiu, Y. (2020). Simulated development and optimized performance of CsPbI3 based all-inorganic perovskite solar cells. *Solar Energy*, *198*, 454-460.

Lin, Q., Kubicki, D. J., Omrani, M., Alam, F., & Abdi-Jalebi, M. (2023). The race between complicated multiple cation/anion compositions and stabilization of FAPbI 3 for halide perovskite solar cells. *Journal of Materials Chemistry C*, *11*(7), 2449-2468.

Liu, G., Zheng, H., Xu, H., Zhang, L., Xu, X., Xu, S., & Pan, X. (2020). Interface passivation treatment by halogenated low-dimensional perovskites for high-performance and stable perovskite photovoltaics. *Nano Energy*, *73*, 104753.

Liu, M., Guo, X., Liu, N., Jiang, C., Zhang, J., Chen, Z., & Zhong, Y. (2025). In-Situ Formation of Low-Dimensional Perovskite Structure for Efficient Single-Crystal MAPbI3 Solar Cells with Enhanced Ambient Stability. *Journal of Materials Chemistry C*.

Liu, Y., Akin, S., Pan, L., Uchida, R., Arora, N., Milić, J. V., Hinderhofer, A., Schreiber, F., Uhl, A. R., & Zakeeruddin, S. M. (2019). Ultrahydrophobic 3D/2D fluoroarene bilayer-based water-resistant perovskite solar cells with efficiencies exceeding 22%. *Science advances*, *5*(6), eaaw2543.

Luan, Y., Wang, F., Zhuang, J., Lin, T., Wei, Y., Chen, N., Zhang, Y., Wang, F., Yu, P., & Mao, L. (2021). Dual-function interface engineering for efficient perovskite solar cells. *EcoMat*, *3*(2), e12092.

Luo, D., Su, R., Zhang, W., Gong, Q., & Zhu, R. (2020). Minimizing non-radiative recombination losses in perovskite solar cells. *Nature Reviews Materials*, *5*(1), 44-60.

Ma, Y., Wang, Y., Fang, Y., Jiang, Y., Dai, Z., & Miao, J. (2024). Recent Advances in the A-Site Cation Engineering of Lead Halide Perovskites. *Advanced Optical Materials*, *12*(30), 2401367.

Man, G. J., Kamal, C., Kalinko, A., Phuyal, D., Acharya, J., Mukherjee, S., Nayak, P. K., Rensmo, H., Odelius, M., & Butorin, S. M. (2022). A-site cation influence on the conduction band of lead bromide perovskites. *Nature communications*, *13*(1), 3839.

Mannar, S., Mandal, P., Roy, A., & Viswanatha, R. (2022). Experimental determination of the molar absorption coefficient of cesium lead halide perovskite quantum dots. *The journal of physical chemistry letters*, *13*(27), 6290-6297.

Mazumdar, S., Zhao, Y., & Zhang, X. (2021). Stability of perovskite solar cells: Degradation mechanisms and remedies. *Frontiers in Electronics*, *2*, 712785.

Miah, M. H., Khandaker, M. U., Rahman, M. B., Nur-E-Alam, M., & Islam, M. A. (2024). Band gap tuning of perovskite solar cells for enhancing the efficiency and stability: issues and prospects. *RSC advances*, *14*(23), 15876-15906.

Njenga, N., & Phiri, T. K. (2024). Ethiopia: Zero-Carbon Energy Systems and Energy Transitions. In *The Palgrave Handbook of Zero Carbon Energy Systems and Energy Transitions* (pp. 409-435). Springer.

Pan, H., Shao, H., Zhang, X. L., Shen, Y., & Wang, M. (2021). Interface engineering for high-efficiency perovskite solar cells. *Journal of Applied Physics*, *129*(13).

Passi, M., & Pal, B. (2021). A review on CaTiO3 photocatalyst: Activity enhancement methods and photocatalytic applications. *Powder Technology*, *388*, 274-304.

Pitchaiya, S., Natarajan, M., Santhanam, A., Asokan, V., Yuvapragasam, A., Ramakrishnan, V. M., Palanisamy, S. E., Sundaram, S., & Velauthapillai, D. (2020). A review on the classification of organic/inorganic/carbonaceous hole transporting materials for perovskite solar cell application. *Arabian Journal of Chemistry*, *13*(1), 2526-2557.

Polo, A. (2021). TERNARY OXIDE SEMICONDUCTOR PHOTOANODES FOR SOLAR ENERGY CONVERSION.

Principe, J., Duarte, V. C., & Andrade, L. (2022). Inverted perovskite solar cells: the emergence of a highly stable and efficient architecture. *Energy Technology*, *10*(4), 2100952.

Priyadarshini, P., Senapati, S., & Naik, R. (2023). Lead-free organic inorganic hybrid halide perovskites: An emerging candidate for bifunctional applications. *Renewable and Sustainable Energy Reviews*, *186*, 113649.

RaeisianAsl, M., Panahi, S. F. K., Jamaati, M., & Tafreshi, S. S. (2022). A review on theoretical studies of structural and optoelectronic properties of FA-based perovskite materials with a focus on FAPbI3. *International Journal of Energy Research*, *46*(10), 13117-13151.

Rahman, M. Z., Edvinsson, T., & Gascon, J. (2022). Hole utilization in solar hydrogen production. *Nature Reviews Chemistry*, *6*(4), 243-258.

Roy, P., Kumar Sinha, N., Tiwari, S., & Khare, A. (2020). A review on perovskite solar cells: Evolution of architecture, fabrication techniques, commercialization issues and status. *Solar Energy*, *198*, 665-688. https://doi.org/https://doi.org/10.1016/j.solener.2020.01.080

Seid, B. A., Sarisozen, S., Peña-Camargo, F., Ozen, S., Gutierrez-Partida, E., Solano, E., Steele, J. A., Stolterfoht, M., Neher, D., & Lang, F. (2024). Understanding and Mitigating Atomic Oxygen-Induced Degradation of Perovskite Solar Cells for Near-Earth Space Applications. *Small*, *20*(30), 2311097.

Seshaiah, K. V., & Kim, J. H. (2024). Nature of defects and their passivation engineering for advancements in perovskite solar cells. *Chemical Engineering Journal*, 152370.

Shah, N., Shah, A., Leung, P., Khan, S., Sun, K., Zhu, X., & Liao, Q. (2023). A review of third generation solar cells. *Processes*, *11*(6), 1852.

Sharma, R., Sharma, A., Agarwal, S., & Dhaka, M. (2022). Stability and efficiency issues, solutions and advancements in perovskite solar cells: A review. *Solar Energy*, *244*, 516-535.

Shi, H., Xie, T., Li, D., Li, Z., Chen, Z., Wang, C., Huang, S., Zheng, F., & Chi, D. (2024). Defect passivation engineering for achieving 4.29% light utilization efficiency MA-free wide-bandgap semi-transparent perovskite solar cells. *Chemical Engineering Journal*, *500*, 156962.

Shi, Y., Rojas-Gatjens, E., Wang, J., Pothoof, J., Giridharagopal, R., Ho, K., Jiang, F., Taddei, M., Yang, Z., & Sanehira, E. M. (2022). (3-Aminopropyl) trimethoxysilane surface passivation improves perovskite solar cell performance by reducing surface recombination velocity. *ACS Energy Letters*, *7*(11), 4081-4088.

Shockley, W., & Queisser, H. J. (1961). Detailed balance limit of efficiency of p-n junction solar cells. *Journal of Applied Physics*, *32*(3), 510-519.

Siegrist, S., Yang, S.-C., Gilshtein, E., Sun, X., Tiwari, A. N., & Fu, F. (2021). Triple-cation perovskite solar cells fabricated by a hybrid PVD/blade coating process using green solvents. *Journal of Materials Chemistry A*, *9*(47), 26680-26687.

Singh, R. (2019). *Electronic and thermal transport properties of engineered organic-inorganic halide perovskite structures* Iowa State University].

Singh, R., Sandhu, S., Yadav, H., & Lee, J.-J. (2019). Stable triple-cation (Cs+–MA+–FA+) perovskite powder formation under ambient conditions for hysteresis-free high-efficiency solar cells. *ACS applied materials & interfaces*, *11*(33), 29941-29949.

Steirer, K., Schulz, P., Teeter, G., Stevanovic, V., Yang, M., Zhu, K., & Berry, J. Defect Tolerance in Methylammonium Lead Triiodide Perovskite, ACS Energy Lett. 1 (2016) 360–366. In.

Subudhi, P., & Punetha, D. (2023). Pivotal avenue for hybrid electron transport layer-based perovskite solar cells with improved efficiency. *Scientific reports*, *13*(1), 19485.

Swarnkar, A., Marshall, A. R., Sanehira, E. M., Chernomordik, B. D., Moore, D. T., Christians, J. A., Chakrabarti, T., & Luther, J. M. (2016). Quantum dot–induced phase stabilization of α-CsPbI3 perovskite for high-efficiency photovoltaics. *Science*, *354*(6308), 92-95.

Taddei, M., Contreras, H., Doan, H.-N., McCarthy, D. P., Seo, S., Westbrook, R. J., Graham, D. J., Datta, K., Carroy, P., & Muñoz, D. (2024). Diamine Surface Passivation and Post-Annealing Enhance Performance of Silicon-Perovskite Tandem Solar Cells. *arXiv preprint arXiv:2411.18756*.

Tao, J., Zhao, C., Wang, Z., Chen, Y., Zang, L., Yang, G., Bai, Y., & Chu, J. (2024). Suppressing non-radiative recombination for efficient and stable perovskite solar cells. *Energy & Environmental Science*.

Tao, J., Zhao, C., Wang, Z., Chen, Y., Zang, L., Yang, G., Bai, Y., & Chu, J. (2025). Suppressing non-radiative recombination for efficient and stable perovskite solar cells. *Energy & Environmental Science*, *18*(2), 509-544.

Teale, S., Degani, M., Chen, B., Sargent, E. H., & Grancini, G. (2024). Molecular cation and low-dimensional perovskite surface passivation in perovskite solar cells. *Nature Energy*, *9*(7), 779-792.

Tegegne, N. (2018). *Photophysics and photovoltaic application of direct heteroarylation derived isoindigo based copolymers* Stellenbosch: Stellenbosch University].

Tien, C.-H., Lin, W.-C., & Chen, L.-C. (2022). Efficient perovskite solar cells via phenethylamine iodide cation-modified hole transport layer/perovskite interface. *ACS omega*, *7*(42), 37359-37368.

Tiep, N. H., Ku, Z., & Fan, H. J. (2016). Recent advances in improving the stability of perovskite solar cells. *Advanced Energy Materials*, *6*(3), 1501420.

Tong, Y., Najar, A., Wang, L., Liu, L., Du, M., Yang, J., Li, J., Wang, K., & Liu, S. (2022). Wide-bandgap organic–inorganic lead halide perovskite solar cells. *Advanced Science*, *9*(14), 2105085.

Vasilopoulou, M., Mohd Yusoff, A. R. B., & Nazeeruddin, M. K. (2023). Perovskite Materials and Perovskite Solar Cells. *Printable Mesoscopic Perovskite Solar Cells*, 137-165.

Wang, M., Lu, Y., Huo, X., Cai, Q., Yao, Y., Zhang, Y., Song, D., Xu, Z., Chen, S., & Chen, G. (2023). Mitigating lattice strain and phase segregation of mixed-halide perovskite films via dual chloride additive strategy toward highly efficient and stable perovskite solar cells. *Journal of Power Sources*, *561*, 232753.

Wang, R., Mujahid, M., Duan, Y., Wang, Z. K., Xue, J., & Yang, Y. (2019). A review of perovskites solar cell stability. *Advanced Functional Materials*, *29*(47), 1808843.

Wang, S., Sang, H., Jiang, Y., Wang, Y., Xiong, Y., Yu, Y., He, R., Chen, B., Zhao, X., & Liu, Y. (2021). Tailoring the energy band structure and interfacial morphology of the ETL via controllable nanocluster size achieves high-performance planar perovskite solar cells. *ACS applied materials & interfaces*, *13*(41), 48555-48568.

Wang, S., Wang, A., Deng, X., Xie, L., Xiao, A., Li, C., Xiang, Y., Li, T., Ding, L., & Hao, F. (2020). Lewis acid/base approach for efficacious defect passivation in perovskite solar cells. *Journal of Materials Chemistry A*, *8*(25), 12201-12225.

Wang, Y., Zhao, H., Piotrowski, M., Han, X., Ge, Z., Dong, L., Wang, C., Pinisetty, S. K., Balguri, P. K., & Bandela, A. K. (2022). Cesium lead iodide perovskites: optically active crystal phase stability to surface engineering. *Micromachines*, *13*(8), 1318.

Wang, Z., Lin, Q., Chmiel, F. P., Sakai, N., Herz, L. M., & Snaith, H. J. (2017). Efficient ambient-air-stable solar cells with 2D–3D heterostructured butylammonium-caesium-formamidinium lead halide perovskites. *Nature Energy*, *2*(9), 1-10.

Wolff, C. M., Caprioglio, P., Stolterfoht, M., & Neher, D. (2019). Nonradiative recombination in perovskite solar cells: the role of interfaces. *Advanced Materials*, *31*(52), 1902762.

Wu, G., Liang, R., Ge, M., Sun, G., Zhang, Y., & Xing, G. (2022). Surface passivation using 2D perovskites toward efficient and stable perovskite solar cells. *Advanced Materials*, *34*(8), 2105635.

Wu, P., Li, D., Wang, S., & Zhang, F. (2023). Magic guanidinium cations in perovskite solar cells: from bulk to interface. *Materials Chemistry Frontiers*, *7*(13), 2507-2527.

Xie, X., Zeng, S., Zhou, C., & Xiao, S. (2023). Fabrication strategies for high quality halide perovskite films in solar cells. *Materials Chemistry Frontiers*, *7*(21), 5309-5332.

Xue, J., Fujitsuka, M., Tachikawa, T., Bao, J., & Majima, T. (2024). Charge trapping in semiconductor photocatalysts: a time-and space-domain perspective. *Journal of the American Chemical Society*, *146*(13), 8787-8799.

Yang, B., Bogachuk, D., Suo, J., Wagner, L., Kim, H., Lim, J., Hinsch, A., Boschloo, G., Nazeeruddin, M. K., & Hagfeldt, A. (2022). Strain effects on halide perovskite solar cells. *Chemical Society Reviews*, *51*(17), 7509-7530.

Yang, D., Zhao, B., Yang, T., Lai, R., Lan, D., Friend, R. H., & Di, D. (2022). Toward stable and efficient perovskite light-emitting diodes. *Advanced Functional Materials*, *32*(9), 2109495.

Yang, M., Zeng, Y., Li, Z., Kim, D. H., Jiang, C.-S., Van De Lagemaat, J., & Zhu, K. (2017). Do grain boundaries dominate non-radiative recombination in CH 3 NH 3 PbI 3 perovskite thin films? *Physical Chemistry Chemical Physics*, *19*(7), 5043-5050.

Yang, W., Su, R., Luo, D., Hu, Q., Zhang, F., Xu, Z., Wang, Z., Tang, J., Lv, Z., & Yang, X. (2020). Surface modification induced by perovskite quantum dots for triple-cation perovskite solar cells. *Nano Energy*, *67*, 104189.

Yao, H., Zhao, J., Li, Z., Ci, Z., & Jin, Z. (2021). Research and progress of black metastable phase CsPbI 3 solar cells. *Materials Chemistry Frontiers*, *5*(3), 1221-1235.

Yao, Z., Zhao, W., & Liu, S. F. (2021). Stability of the CsPbI 3 perovskite: from fundamentals to improvements. *Journal of Materials Chemistry A*, *9*(18), 11124-11144.

Yi, Z. (2021). *Stability study in lead-halide perovskite light-emitting diodes*

Yoo, J. J., Wieghold, S., Sponseller, M. C., Chua, M. R., Bertram, S. N., Hartono, N. T. P., Tresback, J. S., Hansen, E. C., Correa-Baena, J.-P., & Bulović, V. (2019). An interface stabilized perovskite solar cell with high stabilized efficiency and low voltage loss. *Energy & Environmental Science*, *12*(7), 2192-2199.

Yu, D., Wei, Q., Li, H., Xie, J., Jiang, X., Pan, T., Wang, H., Pan, M., Zhou, W., & Liu, W. (2022). Quasi-2D Bilayer Surface Passivation for High Efficiency Narrow Bandgap Perovskite Solar Cells. *Angewandte Chemie*, *134*(20), e202202346.

Yun, S., Qin, Y., Uhl, A. R., Vlachopoulos, N., Yin, M., Li, D., Han, X., & Hagfeldt, A. (2018). New-generation integrated devices based on dye-sensitized and perovskite solar cells. *Energy & Environmental Science*, *11*(3), 476-526.

Zhai, H., Liao, F., Song, Z., Ou, B., Li, D., Xie, D., Sun, H., Xu, L., Cui, C., & Zhao, Y. (2021). 2D PEA2PbI4–3D MAPbI3 Composite perovskite interfacial layer for highly efficient and stable mixed-ion perovskite solar cells. *ACS Applied Energy Materials*, *4*(12), 13482-13491.

Zhang, Y., & Park, N.-G. (2022). Quasi-two-dimensional perovskite solar cells with efficiency exceeding 22%. *ACS Energy Letters*, *7*(2), 757-765.

Zhao, Y., Zhou, W., Han, Z., Yu, D., & Zhao, Q. (2021). Effects of ion migration and improvement strategies for the operational stability of perovskite solar cells. *Physical Chemistry Chemical Physics*, *23*(1), 94-106.

Zheng, L., Owor, R. S., & Li, Z. (2019). Environmentally Benign All-inorganic Perovskite Solar Cells. *Advances in Materials*, *8*(4), 142.

Zhou, C., Tarasov, A. B., Goodilin, E. A., Chen, P., Wang, H., & Chen, Q. (2022). Recent strategies to improve moisture stability in metal halide perovskites materials and devices. *Journal of energy chemistry*, *65*, 219-235.

Zhou, K., Qi, B., Liu, Z., Wang, X., Sun, Y., & Zhang, L. (2024). Advanced organic–inorganic hybrid materials for optoelectronic applications. *Advanced Functional Materials*, *34*(52), 2411671.

Zhou, Q., Karani, A., Lian, Y., Zhao, B., Friend, R. H., & Di, D. (2021). Photonically-confined solar cells: prospects for exceeding the Shockley-Queisser limit. *arXiv preprint arXiv:2106.04391*.

Zhou, T., Lai, H., Liu, T., Lu, D., Wan, X., Zhang, X., Liu, Y., & Chen, Y. (2019). Highly efficient and stable solar cells based on crystalline oriented 2D/3D hybrid perovskite. *Advanced Materials*, *31*(32), 1901242.

Zhou, Y., Eck, M., & Krüger, M. (2010). Bulk-heterojunction hybrid solar cells based on colloidal nanocrystals and conjugated polymers. *Energy & Environmental Science*, *3*(12), 1851-1864.

Zhu, H., Teale, S., Lintangpradipto, M. N., Mahesh, S., Chen, B., McGehee, M. D., Sargent, E. H., & Bakr, O. M. (2023). Long-term operating stability in perovskite photovoltaics. *Nature Reviews Materials*, *8*(9), 569-586.

Zhuang, J., Mao, P., Luan, Y., Yi, X., Tu, Z., Zhang, Y., Yi, Y., Wei, Y., Chen, N., & Lin, T. (2019). Interfacial passivation for perovskite solar cells: the effects of the functional group in phenethylammonium iodide. *ACS Energy Letters*, *4*(12), 2913-2921.

Zhukovskiy, Y. L., Batueva, D. E., Buldysko, A. D., Gil, B., & Starshaia, V. V. (2021). Fossil energy in the framework of sustainable development: analysis of prospects and development of forecast scenarios. *Energies*, *14*(17), 5268.